Title: MLT-11 is a transient apical extracellular matrix component required for cuticle patterning and function

James Matthew Ragle[1], Ariela Turzo[1], Max T. Levenson[1], Keya Jonnalagadda[1], Anton Jackson[1], An A. Vo[1], Vivian T. Pham[1] and Jordan D. Ward[1‡].

[1]Department of Molecular, Cell, and Developmental Biology, University of California-Santa Cruz, Santa Cruz, CA 95064, USA.

[‡]Author for correspondence.

Corresponding author email: jward2@ucsc.edu

Keywords: *C. elegans*, molting, Kunitz domain, apical extracellular matrix, protease inhibitor

Running Title: MLT-11 and *C. elegans* development

ABSTRACT

Apical extracellular matrices (aECMs) are associated with all epithelia and form a protective layer against biotic and abiotic threats in the environment. Despite their importance, we lack a deep understanding of their structure and dynamics in development and disease. *C. elegans* molting offers a powerful entry point to understanding developmentally programmed aECM remodeling. A transient matrix is formed in embryos and at the end of each larval stage, presumably to pattern the new cuticle. Focusing on targets of NHR-23, a key transcription factor which drives molting, we identified the Kunitz family protease inhibitor gene *mlt-11* as an NHR-23 target. We identified NHR-23-binding sites that are necessary and sufficient for epithelial expression. *mlt-11* is necessary to pattern every layer of the adult cuticle, suggesting a broad patterning role prior to the formation of the mature cuticle. MLT-11::mNeonGreen::3xFLAG transiently localized to the aECM in the cuticle and embryo. It was also detected in lining openings to the exterior (vulva, rectum, mouth). Reduction of *mlt-11* function disrupted the barrier function of the cuticle. Tissue-specific RNAi suggested *mlt-11* activity is primarily necessary in seam cells and we observed alae and seam cell fusion defects upon *mlt-11* inactivation. Predicted *mlt-11* null mutations caused fully penetrant embryonic lethality and elongation defects suggesting *mlt-11* also plays an important role in patterning the embryonic sheath. Finally, we found that *mlt-11* inactivation suppressed the blistered cuticle phenotype of mutants of *bli-4* mutants, a subtilisin protease gene but did not affect BLI-4::sfGFP expression. These data could suggest that MLT-11 may be necessary to assure proper levels of BLI-4 activity.

INTRODUCTION

Specialized extracellular matrices cover the apical surface of all epithelial cells and form the skin in almost all animals [1–3]. These apical extracellular matrices (aECMs) also line the lumen of internal tubular epithelia to form a protective layer against biotic and abiotic threats [1–3]. Despite their importance, understanding the structure and dynamics of aECM components in development and disease remains challenging.

C. elegans is emerging as a powerful model to study aECM structure and remodeling. They have a collagen-based aECM (cuticle) so understanding its assembly may provide insight into mammalian skin biology [4]. The components of the cuticle are secreted by hypodermal and seam cells and are assembled in distinct layers [4–6]. The cuticle secreted by the hypodermal syncytium form circumferential ridges called annuli separated from one another by furrows [4]. In adults an inner basal layer contains two fibrous sub-layers angled in opposite directions and an outer cortical layer [5]. A fluid-filled medial layer contains hollow, nano-scale struts built from the BLI-1 and BLI-2 collagens [5,7]. All layers are composed of extensively cross-linked collagens. The cortical layer also contains cuticlins, proteins which remain in the insoluble fraction after cuticle solubilization [8]. The cortical layer is covered by the epicuticle, a poorly understood structure that is thought to be a lipid bilayer covered by a glycoprotein rich surface coat [9–11]. There can be stage-specific variations in cuticle structure. Only adults have a medial layer, and both L1 and adult cuticles contain alae, lateral longitudinal ridges secreted by seam cells in the epidermis [5,12].

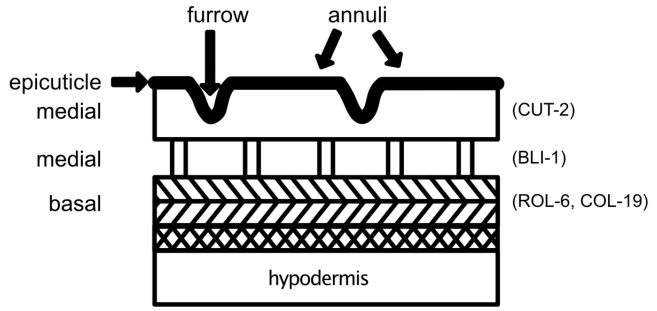

Fig. 1. The *C. elegans* adult cuticle has multiple layers with unique structures and collagen content. Cartoon model of the *C. elegans* adult cuticle sublayers (epicuticle, cortical, medial and basal), topological features (annuli and furrows). The localization of proteins used to mark specific layers of the cuticle in this study is indicated (CUT-2, BLI-1, ROL-6 and COL-19)[7,8,49].

During each larval stage animals must build a new aECM underneath the old one and separate the old aECM (apolysis) that is subsequently shed (ecdysis) [13]. A specialized, transient structure known as the pre-cuticle is thought to pattern the new cuticle and is then endocytosed [14]. Pre-cuticle components include zona pellucida proteins, lipocalins, fibrillin, extracellular leucine-rich repeat proteins, and hedgehog-related proteins [14–19]. The sheath is a similar structure in embryos which ensures embryonic membrane integrity and directs force during elongation [20–23]. The vulval aECM has recently been shown to be highly dynamic, and specialized aECMs also line the rectum and excretory system [15,16,24].

A major question is how is the new aECM constructed and the old one shed during molting? A poorly understood genetic oscillator is thought to coordinate the expression of cuticle components and processing enzymes [25,26]. The molting cycle must also be tightly linked to developmental progression with homologs of circadian rhythm proteins (LIN-42/PER, NHR-23/ROR) playing important roles in both the molting and developmental timers [27–36]. Study of NHR-23-regulated genes revealed an enrichment in predicted protease and protease inhibitors [32,33]. Proteases are required for molting or ecdysis in both *C. elegans* and parasitic nematodes, presumably by promoting apolysis, though some are thought to function in collagen processing [37–44]. Protease inhibitors have been implicated in molting through RNAi screening, and have been suggested to suppress ecdysis [13,44,45]. MLT-11 is a predicted protease inhibitor in the Kunitz family and *mlt-11 (RNAi)* causes molting defects [44]. *mlt-11* mRNA oscillates, peaking mid-molt and its expression is regulated by NHR-23, yet *mlt-11* remains poorly characterized [25,26,31–35,44].

Here we show that MLT-11 is secreted and transiently localizes to the aECM over the hypodermis and seam cells, before being endocytosed. It also localizes to the rectal epithelium, excretory duct lumen, and vulval lumen. Reduction of *mlt-11* function in larvae causes developmental delay, failure to apolyse and a loss of the cuticle barrier function. Additionally, cuticle collagens in each layer of the mature adult cuticle are aberrantly localized suggesting *mlt-11* has a broad role in patterning the developing cuticle. *mlt-11* activity in seam cells is necessary for molting and a normal developmental rate. Like embryonic sheath components, it is secreted into the extracellular space and surrounds the exterior of the embryo before being endocytosed prior to hatching. *mlt-11* null alleles cause embryonic lethality, characterized by disorganization of adherens junctions. *mlt-11* inactivation suppresses the blistered cuticle phenotypes in mutants of the subtilisin/kexin (PCSK) family protease, *bli-4*. Together, this work provides the first insight into how MLT-11 functions to promote embryogenesis and aECM integrity during molting. Our identification of BLI-4 as a potential MLT-11 substrate is an entry point into understanding mechanistically how MLT-11 promotes molting.

RESULTS

Multiple NHR-23 occupied genomic regions regulate *mlt-11* expression

Our previous study found an enrichment in protease and protease inhibitors in genes regulated by the NHR-23 nuclear hormone receptor transcription factor [32]. *mlt-11* is a poorly characterized predicted protease inhibitor that is *nhr-23*-regulated with four NHR-23 ChIP-seq peaks upstream of its transcriptional start site [32,33,44,46]. Consistent with potential direct NHR-23 binding to these regions, there are GGGTCA or AGGTCA half sites that NHR-23 binds *in vitro* (Fig. 2A)[35]. To determine the contribution of these NHR-23 occupied regions to *mlt-11* expression we turned to promoter reporters. We first created a single-copy *mlt-11p::NLS::mNeonGreen* promoter reporter including the sequences of peaks 1-3 (-2.8 kb *mlt-11p*) (Fig. 2A). Similar to a previous promoter reporter study [44], we observed mNeonGreen expression in hypodermal and seam cells, as well as novel expression in the developing rectal and vulval epithelial cells, and developing embryo (Fig. 2B,C). Expression in embryos was first detected at the bean stage in posterior epithelial cells and persisted through the 3-fold stage and expression spread anteriorly (Fig. 2C). The previously characterized *mlt-11* promoter reporter contained the the sequence of peak 3 and part of peak 4 [44], but lacked the sequences from peaks 1 and 2 . We therefore generated an equivalent promoter reporter to Frand et al. (2005) as well as a larger promoter fragment (-5.2 kb *mlt-11p*) containing the sequences from peaks 1-4. Similar expression timing and intensity was seen in all three reporters (Fig. 2D).

Given that the Frand promoter and our -2.8 kb promoter overlapped in the region containing the NHR-23 peak 3 sequences, we hypothesized that this region may play a key role in regulating *mlt-11* expression. We therefore tested whether the sequence contained in each NHR-23 ChIP-seq peak, as well as two candidate enhancers identified by ATAC-seq were sufficient to drive the expression of a reporter containing a *pes-10* minimal promoter. This reporter displays undetectable mNG expression in the absence of an additional *cis*-regulatory element (Fig. 2E). We detected reporter expression containing peaks 3 and 4 in hypodermal cells with peak 3 being the most robust (Fig. 2E). Additionally, we detected expression in seam cells with the regulatory element from peaks

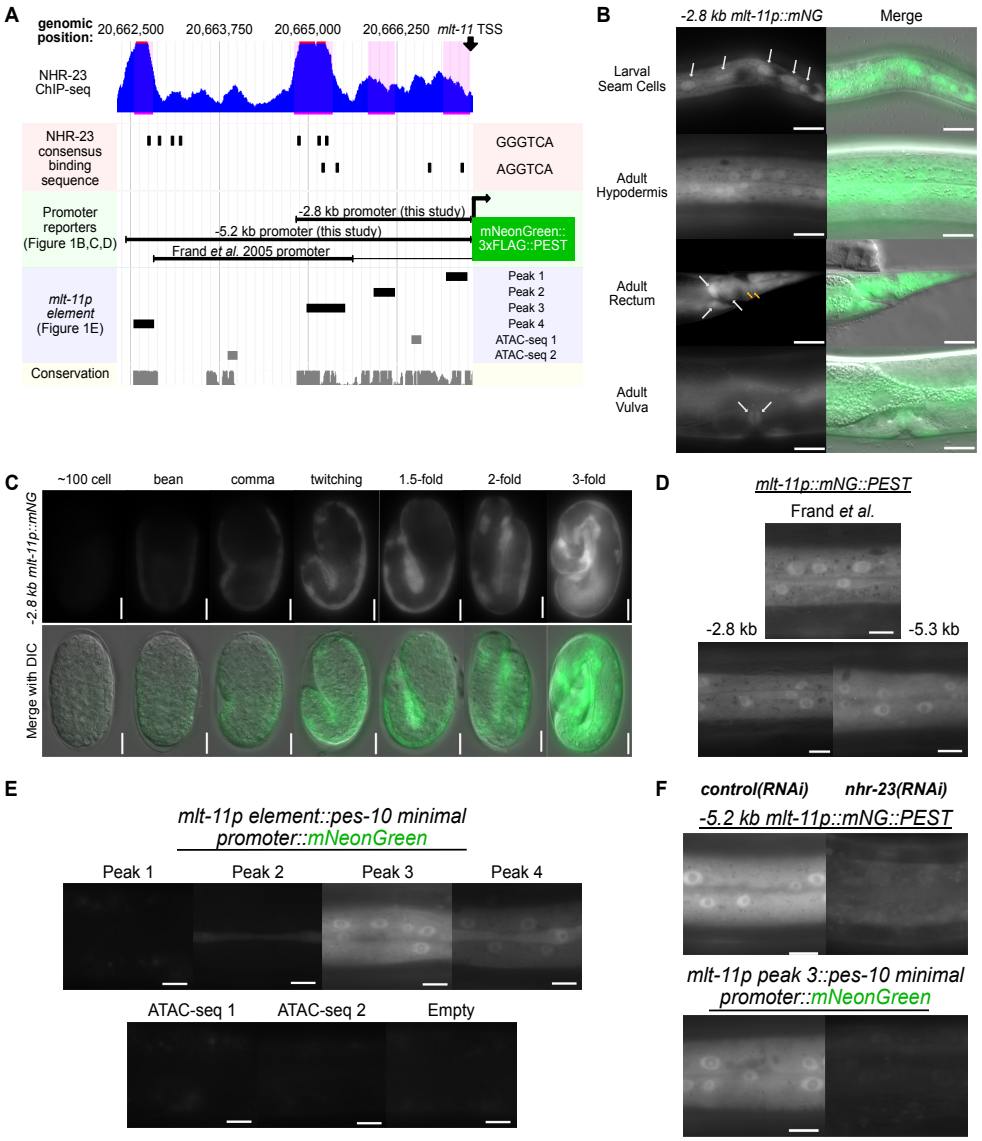

Fig. 2. *mlt-11* is expressed in larval and embryonic epidermal cells. (A) Genome browser track of *mlt-11* promoter depicting NHR-23 ChIP-seq peaks; relative genomic locations of NHR-23 binding motifs; relative genomic locations of *mlt-11* promoter reporters used in this study; relative genomic locations of candidate *cis*-regulatory elements from the *mlt-11* promoter inserted into a *pes-10* minimal promoter in this study; conservation calculated across 26 nematode species. (B) Expression pattern of a *-2.8kb mlt-11p::mNG::tbb-2 3'UTR* promoter reporter in hypodermal cells of L4 worms. White arrows indicate seam cells (top), rectal epithelial cells (middle) and vulval cells (bottom) and yellow arrows indicate hypodermal cells near rectum. Images are representative of 40 animals examined over two biological replicates. (C) Time course of *-2.8kb mlt-11p::mNG::tbb-2 3'UTR* expression in embryos with stages determined by embryo morphology. (D) Hypodermal expression pattern in L4s of three single-copy integrated promoter reporters. One reporter uses the same sequence used by Frand *et al.* (2005) and the other two use -2.8 kb and 5.2 kb of sequence upstream of the *mlt-11* transcriptional start site (TSS). (E) Hypodermal expression pattern in L4s of single-copy integrated promoter reporters with the *pes-10* minimal promoter elements combined with *mlt-11* promoter sequence fragments corresponding to either NHR-23 ChIP-seq or peaks or ATAC-seq open chromatin regions. (F) Hypodermal expression pattern in L4 larvae of the indicated single-copy integrated promoter reporters. Reporter strains were fed either control or *nhr-23(RNAi)* knockdown conditions. Scale bars are 20 µm in B, D, E and F and 10 µm in C.

143 2, 3 and 4 (Fig. 2E). We could detect no expression of reporters containing peak 1 nor
144 ATAC-seq 1 or 2 (Fig. 2E). To test whether NHR-23 regulated expression of the *mlt-11*
145 *peak 3 pes-10::mNeonGreen* promoter reporter, we performed *nhr-23* RNAi. RNAi of *nhr-*
146 *23* reduced expression of both full length (Fig. 2F) and *mlt-11 peak 3 pes-*
147 *10::mNeonGreen* promoter reporters (Fig. 2F). These data indicate that NHR-23
148 regulates *mlt-11* and that the DNA sequences in NHR-23 ChIP-seq peaks 3 and 4 play
149 an important role in this regulation.
150
151 **MLT-11 transiently localizes to epithelial aECMs**
152 To gain insight into how MLT-11 regulates molting, we analyzed spatiotemporal MLT-11
153 expression using vulval morphology in L4 larvae for precise staging [47]. We knocked an
154 *mNeonGreen::3xFLAG* cassette into the 3' end of the 7th exon producing an internal
155 translational fusion that labels all described *mlt-11* isoforms (Fig. 3A). MLT-
156 11::mNeonGreen::3xFLAG (MLT-11::mNG) was detected internally in punctate and
157 tubular structures in the hypodermis that are likely lysosomal based on previous
158 colocalization studies of a *mlt-11::mScarlet* knock-in and the precuticle component *noah-*
159 *1* (Fig. 3B)[32,48]. MLT-11::mNG is also transiently detected in the aECM of hyp7 and
160 seam cells, first appearing in furrows of the aECM (larval sub-stage L4.3) and then
161 localizing to annuli in L4.5 (Fig. 3B). By L4.9, localization in the aECM diminished beyond
162 observable levels and we only observed internal punctate expression (Fig. 3B). MLT-
163 11::mNG was seen in the aECM of seam cells from early to mid-L4, localizing to alae and
164 then disappeared in stage L4.6, while loss of MLT-11::mNG in the annuli began in stage
165 L4.6 and was absent in the cuticle by stage L4.9. (Fig. 3B). The transient localization of
166 MLT-11 in the cuticle followed by endocytosis is reminiscent of the pre-cuticle component
167 NOAH-1, which we showed to be internalized in late L4 [32]. In the aECM of the
168 developing vulva, MLT-11::mNG was observed faintly beginning at L4.3, intensifying until
169 L4.5 and remaining localized through the end of the L4 larval stage (Fig. 3C). It appeared
170 most intensely in the aECM of the inner vulva, adjacent to vulC, D, E and F (Fig. 3C).
171 MLT-11::mNG was also observed in the epithelial aECM of other external-facing orifices:
172 the buccal cavity, excretory duct and rectum (Fig. 3D-F). Together, these data indicate

173 that MLT-11 lines openings to the exterior and transiently associates with the cuticle
174 aECM, similar to precuticle components [24,32].
175

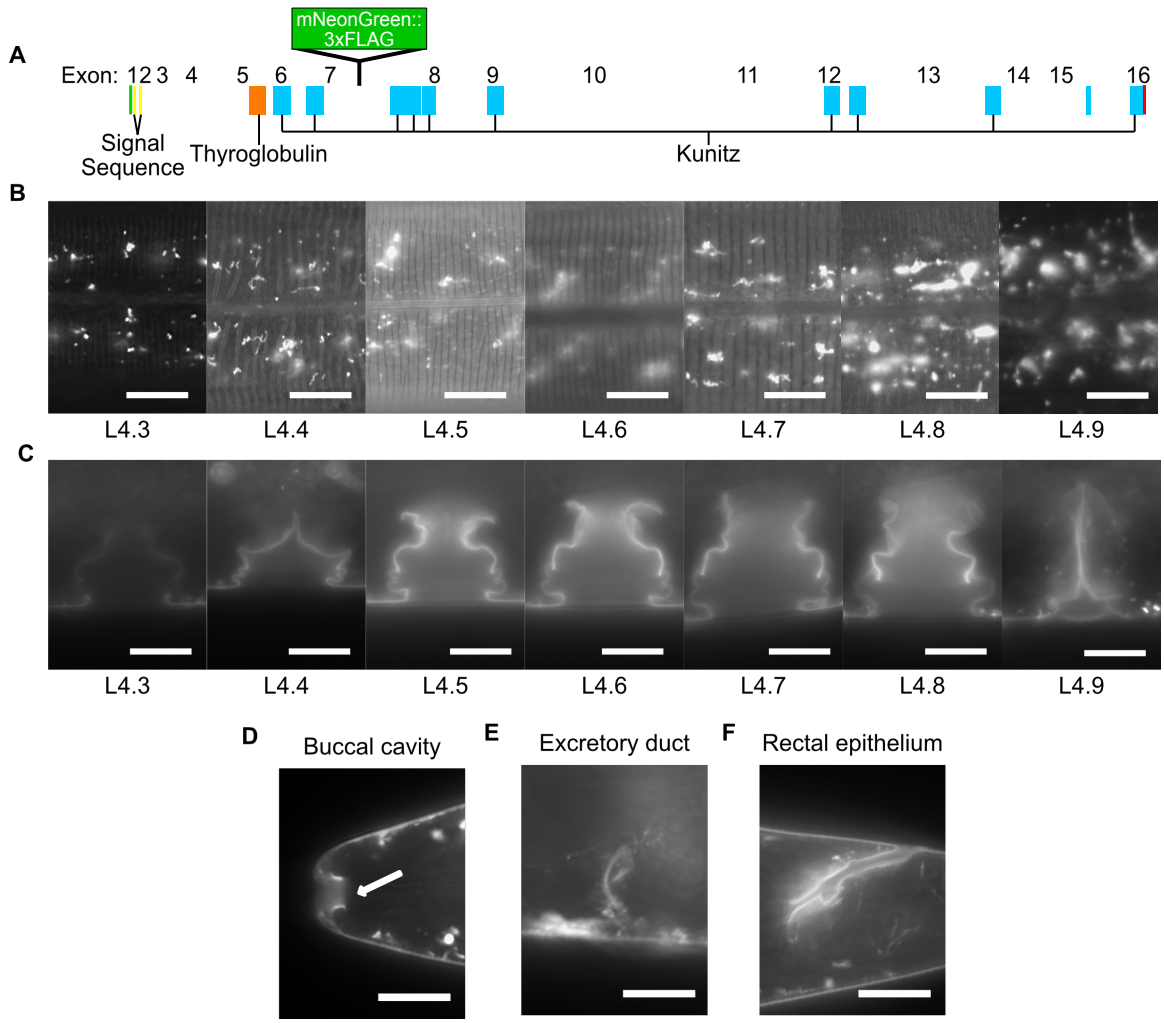

Fig. 3. MLT-11 localizes to the aECM in seam and hypodermal cells and interfacial orifices. (A) Schematic of the interna; *mlt-11::mNG::3xFLAG* knock-in. (B) Developmental time course of MLT-11::mNG in the aECM and internal vesicles of seam and hypodermal cells in the indicated L4 substages. (C) Developmental time course of MLT-11::mNG in the vulva of the indicated L4 substages. (D) Representative images of MLT-11::mNG lining the lumen of the buccal cavity, excretory duct and rectum. Images are representative of 40 animals examined over two biological replicates. Scale bars are 20 µm.

176 ***mlt-11* knockdown causes defective aECM structure and function**

177 Our *mlt-11::mNG* translational fusion strain provided an entry point into understanding
178 how the candidate NHR-23 regulatory elements (Fig. 2) in the *mlt-11* promoter regulate
179 *MLT-11* expression. Using CRISPR/Cas9, we individually deleted the sequence from
180 each NHR-23 ChIP-seq peak (Fig. 4A) in the MLT-11::mNG background and observed

181 expression of the translational fusion. MLT-11::mNG expression was comparable
182 between the control and strains with deletions of peaks 1 or 2 (Fig. 4B). However MLT-
183 11::mNG expression was reduced following deletion of peaks 3 or 4 (Fig. 4B). Deletion
184 of both peaks 3 and 4 in the same strain resulted in severely reduced expression of MLT-
185 11::mNG (Fig. 4B), suggesting that together these sequences are necessary for activation
186 of expression of *mlt-11* by NHR-23. We also scored developmental rate, size, and motility

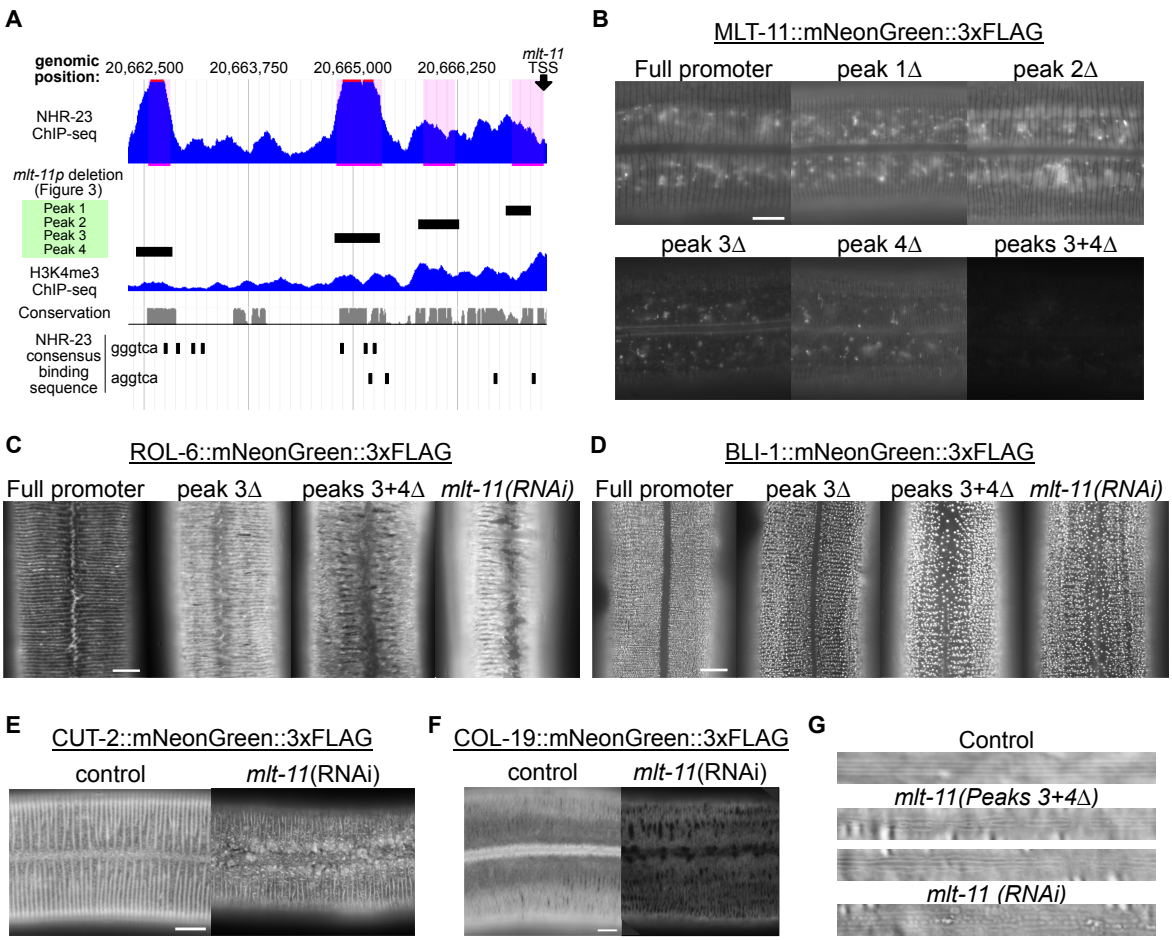

Fig. 4. Disruption of *mlt-11* expression by RNAi or promoter deletion causes abnormalities in cuticle structure. (A) Genome browser track of *mlt-11* promoter depicting NHR-23 ChIP-seq peaks; relative genomic locations of *mlt-11* promoter sequence deletions; an H3K4me3 ChIP-seq track to indicate potential enhancers; conservation calculated across 26 nematode species; relative genomic locations of NHR-23 binding motifs. (B) Representative images of MLT-11::mNG::3xFLAG in mid-stage L4 larvae with endogenous deletion of the indicated promoter regions. (C-F) Representative images of mNG::3xFLAG fused to ROL-6 (C), BLI-1 (D), CUT-2 (E) or COL-19 (F) in the cuticles of mid-stage L4 larvae in control (full promoter) or *mlt-11* expression abrogated (peak 3Δ, peaks 3+4Δ, *mlt-11(RNAi))* backgrounds. (G) (DIC images of adult alae in wild-type animals, *mlt-11(peaks 3+4Δ)* deletion mutants, and *mlt-11(RNAi)* animals. Scale bars are 10 µm in B-F and 5 µm H.

187 (Fig. S1). Interestingly, peak 2 Δ, peak 3+4 Δ and *mlt-11(RNAi)* animals exhibited
188 comparable developmental delay (Fig. S1A), but peak 2Δ animals had wild type motility
189 and size (Fig. S1B, C). In contrast, peak 3+4 Δ and *mlt-11(RNAi)* animals exhibited a
190 significant motility defect with the RNAi causing a stronger phenotype and a comparable
191 smaller body size (Fig. S1B,C).
192

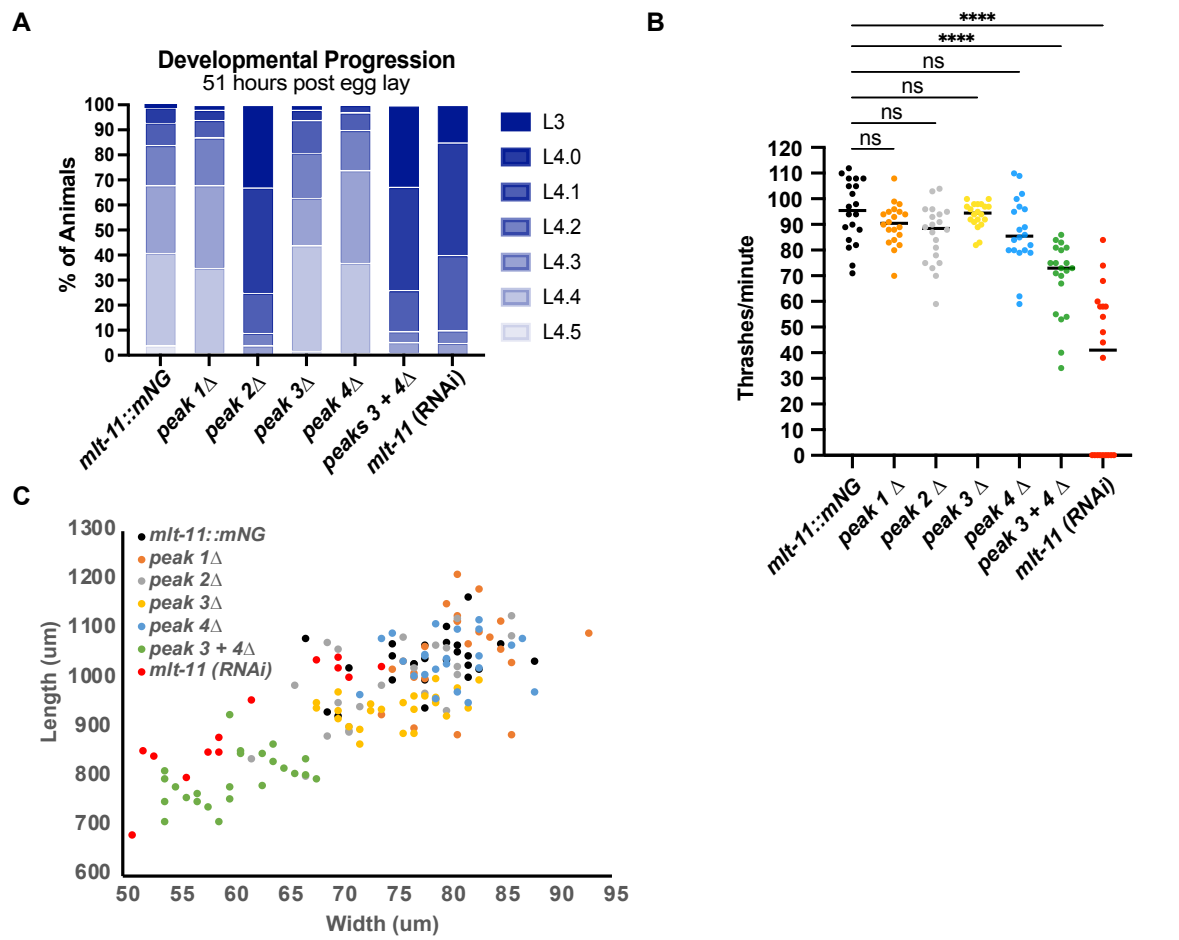

Supplemental Fig. 1. *mlt-11* expression abrogation causes developmental delay, motility defects and smaller bodies. Worms of the indicated genotypes and treatment (control or *mlt-11(RNAi))* were allowed to lay eggs for two hours, then removed from the plates. Embryos were allowed to develop for 51 hours, then scored for (A) developmental stage (L3 or L4 substage), (B) thrashes per minute and (C) body length and width.

193 Given that *mlt-11* expression is regulated by NHR-23 and that NHR-23 depletion causes
194 aECM aberrations, we next wished to see how *mlt-11* inactivation impacted cuticle
195 structure and function. The *C. elegans* cuticle is a complex structure that is composed of
196 multiple layers (Figure 1) [4]. In the adult cuticle, the basal layer is closest to the

197 hypodermis, the cortical layer is furthest from the hypodermis and a fluid-filled medial
198 layer is between them. Each layer contains a unique complement of collagen proteins
199 that provide structure to the cuticle [13]. Given that knockdown of *mlt-11* by RNAi (Frand
200 *et al.*, 2005) causes gross molting defects, we surmised that *mlt-11* could have a role in
201 establishing or maintaining the structure of the cuticle, in apolysis or ecdysis. To test a
202 role in cuticle structure, we depleted *mlt-11* by RNAi or deleted promoter elements in
203 strains carrying translational mNG fusions to proteins that mark the basal layer (ROL-6,
204 COL-19), medial layer (BLI-1), and cortical layer (CUT-2) [7,8,49].
205
206 ROL-6 is a collagen that localizes to tight longitudinal bands (furrows) in the basal layer
207 of the adult cuticle (Fig. 4C)[32,50]. It also resides in patches along the junction of
208 opposing annuli above seam cells (Fig. 4C). Following deletion of peak 3 or peaks 3+4,
209 ROL-6::mNG localized to both furrows and annuli. Gaps were observed between annuli
210 and patches were still seen, but smaller and fewer in number over seam cells. Following
211 RNAi knockdown of *mlt-11*, annuli were separated by larger and more numerous gaps.
212 Localization of ROL-6::mNG was absent over seam cells and opposing annuli at the
213 junction were completely separated from each other and often broken at their termini (Fig.
214 4C). COL-19::mNG, another basal layer marker and adult-specific collagen normally
215 localizes to alae and annuli, but following *mlt-11* RNAi we observed a reduction in
216 expression and a loss of localization over the seam cells (Fig. 4F)[51].
217
218 BLI-1 is a structural collagen found in the medial layer of the adult cuticle, providing
219 connection between the basal and cortical layers in the form of vertical struts [7,52]. BLI-
220 1::mNG localized in punctae organized in circumferential rows across the hyp7 cuticle,
221 but is absent over seam cells (Fig. 4D). Deletion of *mlt-11* peak 3 led to gaps between
222 the rows and inconsistency in the size of punctae (Fig. 4D). Deletion of peaks 3 and 4
223 together or RNAi knockdown caused further disorganization of BLI-1::mNG rows and
224 mislocalization of punctae in seam cuticle (Fig. 4D).
225
226 Similarly, CUT-2, a cuticlin in the cortical layer [8,53], had localization patterns that were
227 altered following knockdown of *mlt-11*. CUT-2::mNG displayed aberrant localization over

228 the seam cells and a fibrous pattern over seam cells following *mlt-11* RNAi (Fig. 4E).
229 Together, this suggests *mlt-11* is necessary for proper formation or patterning of each
230 layer of the adult cuticle.
231
232 Given the aberrant localization of ROL-6, BLI-1, CUT-2, and COL-19 over the seam cells,
233 we next examined alae morphology. The lateral alae are cuticle ridges formed by the
234 interaction between the actin cytoskeleton in epithelial cells and an extracellular
235 provisional matrix [12,54]. Three continuous longitudinal ridges span the midline of lateral
236 surfaces of adult worms (Fig. 4G). Deletion of *mlt-11* peaks 3 and 4 resulted in
237 discontinuous alae. Knockdown of *mlt-11* with RNAi caused the formation of spotty
238 stretches of discontinuous and disorganized alae (Fig. 4G). It is evident that *mlt-11* is
239 necessary for accurate development of cuticle structures derived from both hypodermal
240 and seam cells.
241
242 **Reduced *mlt-11* expression disrupts the cuticle permeability barrier**
243 The cuticle functions as a barrier to protect *C. elegans* from environmental threats such
244 as pathogens and xenobiotics. Gaps and disorganization of multiple layers of the *C.*
245 *elegans* cuticle following *mlt-11* knockdown suggest that this cuticle barrier function may
246 be disrupted, similar to what we observed in NHR-23-depleted animals [32]. To test the
247 cuticle barrier function, we incubated control, promoter deletion mutants and *mlt-11(RNAi)*
248 animals with the cuticle impermeable, cell membrane permeable Hoechst 33258 dye and
249 scored animals with stained nuclei. In wild-type control and single peak deletion animals
250 we observed no Hoechst staining, while we observed staining in 91% of peak 3+4
251 deletion mutants and 93% of *mlt-11(RNAi)* worms (Fig. 5A). This barrier defect was
252 comparable to the *bus-8* positive control strain [55]. Additionally, double deletion of peaks
253 3+4 as well as *mlt-11* RNAi-induced expression of an *nlp-29::GFP* promoter reporter
254 generally activated by infection, acute stress, and physical damage to the cuticle (Fig. 5B)
255 [56,57]. Together, these indicate *mlt-11* is necessary for the barrier function of the cuticle.
256
257
258

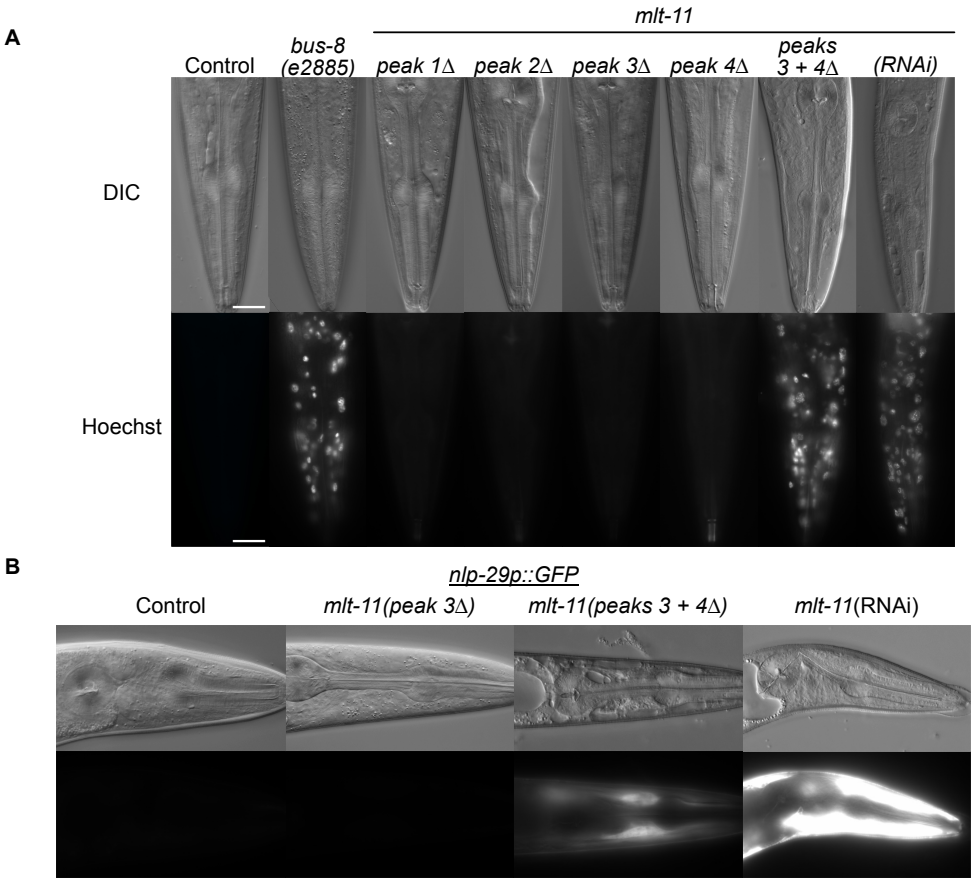

Fig. 5. *mlt-11* knockdown causes defective aECM structure and function. (A,B) Representative images of mid-stage L4 larvae in animals of the indicated genotype/treatment. (A) Worms were washed and incubated with the cuticle impermeable/membrane permeable Hoechst 33258 dye before being imaged. (B) Worms carried an *nlp-29p::GFP* reporter activated by infection, acute stress, and physical damage to the cuticle [56,57]. Three biological replicates were performed and over 40 animals scored. Scale bars are 20 μm.

mlt-11 activity is necessary in seam cells for larval development

As we observed aberrant cuticle protein localization in the aECM over both seam and hypodermal cells, we were curious whether *mlt-11* expressed in these cells may be playing distinct functions and turned to a tissue-specific RNAi approach (Fig. 6A). *mlt-11* knockdown in JDW371, a tissue-specific RNAi strain that restricts knockdown to seam, hypodermal, and intestinal cells [32], phenocopied *mlt-11* RNAi in wildtype animals with respect to developmental delay and molting defects (Fig. 6B-D). *mlt-11* RNAi in QK52, a hypodermal and seam cell-specific RNAi strain, produced less penetrant developmental delay and molting defects (Fig. 6B-D). Notably, *mlt-11* RNAi in a hypodermal-specific

270

A

Strain	Promoter for tissue-specific RNAi	Tissue-specific RNAi	RNAi	N
N2	N/A	whole animal	Control	252
			mlt-11	186
JDW371	*SCMmin*	seam, hyp and intestine	Control	181
			mlt-11	181
JDW510	*semo-1*	hypodermis and intestine	Control	259
			mlt-11	301
QK52	*wrt-2*	seam, hypodermis, rectum	Control	230
			mlt-11	158
VP303	*nhx-2*	intestine	Control	227
			mlt-11	219
JU2039	*lin-31*	vulva precursors	Control	258
			mlt-11	312
WM118	*myo-2*	body muscle	Control	139
			mlt-11	157
MGH171	*vha-6*	intestine	Control	347
			mlt-11	406

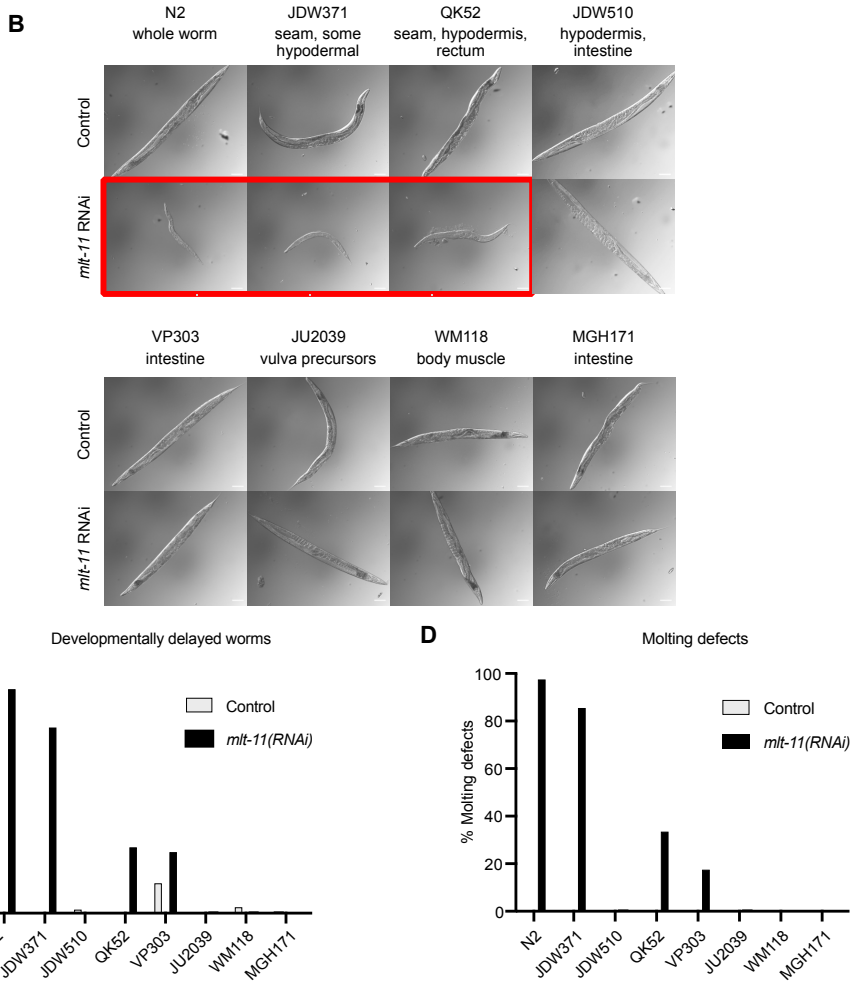

Fig. 6. *mlt-11* is necessary in seam cells for molting and larval development. (A) Tissue-specific RNAi strains used. A timed egg lay of animals of the indicated genotype were performed on control or *mlt-11 (RNAi)* plates and phenotypes were scored three days later. (B) Representative images of animals of the indicated genotype grown on control or *mlt-11* RNAi. The red box highlights conditions that produced smaller larvae with molting defects. (C) Developmental delay was scored in the indicated strains grown on control or *mlt-11* RNAi plates and classified as a failure to reach adulthood after 72 hours of growth. (D) Molting defects were scored in the indicated strains on control or *mlt-11* RNAi. Scored defects included animals dragging cuticles, ecdysis failure and cuticle corsets. Tissue-specific RNAi data is from two independent replicates.

271 RNAi strain, JDW510, produced no developmental delay or molting defects, suggesting
272 *mlt-11* activity is necessary in seam cells and perhaps, in a limited capacity, in other
273 hypodermal cells (Fig. 6B-D).
274

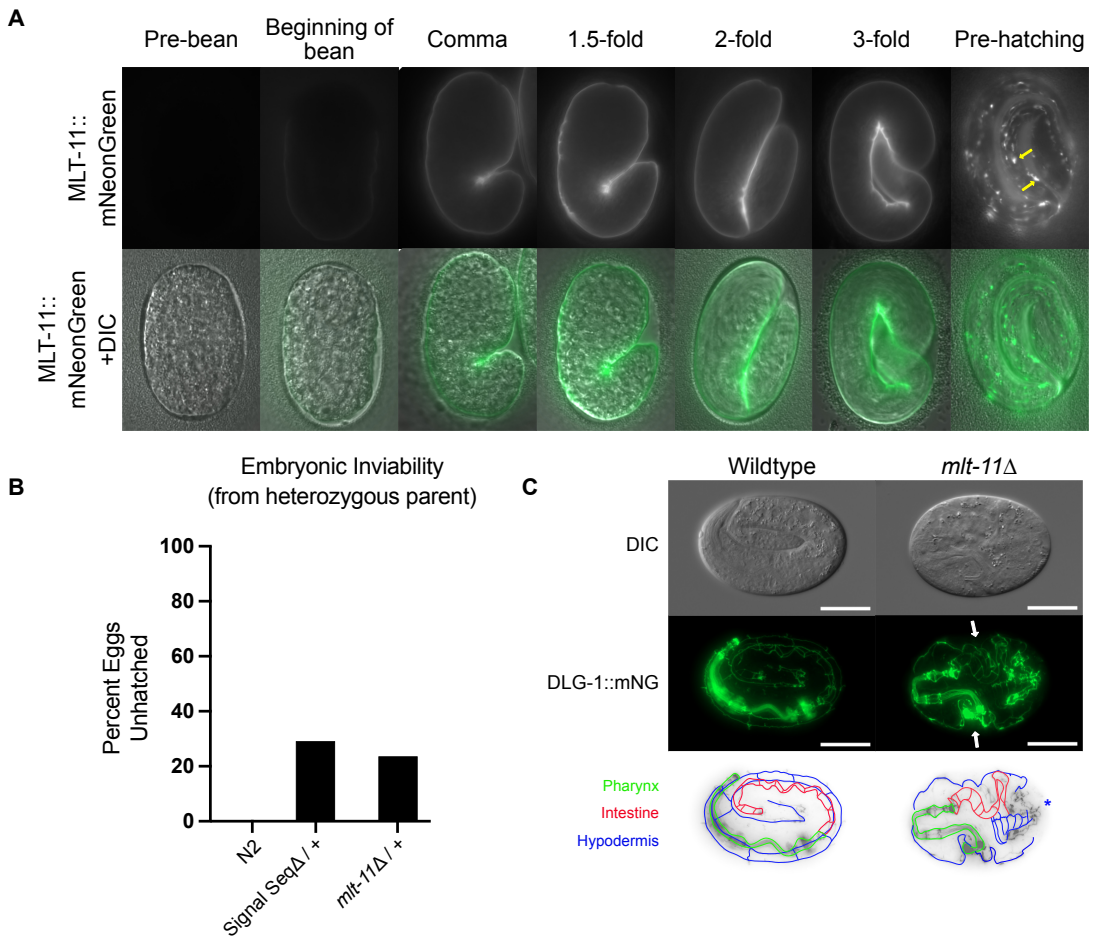

Fig. 7. MLT-11 localizes to the embryonic sheath and is necessary for proper hypodermal development during embryogenesis. (A) Developmental time course of MLT-11::mNG in the aECM and internal vesicles of seam and hypodermal cells in the indicated embryonic substages. Yellow arrows indicate MLT-11::mNG has been endocytosed to internal vesicles at the end of elongation. (B) Endogenous deletions of the signal sequence and Kunitz domains 3-10 (*mlt-11*Δ) are homozygous inviable and so were balanced and maintained as heterozygotes. These heterozygotes were plated as adults and allowed to lay eggs for 2 hours, then removed. The resulting embryos were allowed to develop for 24 hours and then scored for hatching. (C) Representative orthogonal projection of a balanced *mlt-11*Δ heterozygous embryo and a homozygous *mlt-11*Δ embryo expressing DLG-1::mNG labeled adherens junctions in the pharynx, intestine, and hypodermis. White arrows indicate invaginations in the hypodermal cells. Scale bars are 20 µm.

275 ***mlt-11* is a component of the embryonic sheath and is required for elongation**
276 Most of our analyses of *mlt-11* was carried out in L4 larvae as they developed the adult
277 and final cuticle. Abrogation of *mlt-11* expression led to wide-spread cuticle defects

278 suggesting MLT-11 may play a larger role in patterning the cuticle as opposed to being a
279 component of the cuticle itself. Indeed, we never saw MLT-11 shed in the cuticle, rather
280 it was endocytosed, likely to lysosomes (Fig. 3B). This idea is supported by the timing of
281 MLT-11::mNG expression and localization at the intermolt when the pre-cuticle or
282 provisional matrix is present. A similar scenario plays out during embryonic
283 morphogenesis when a ball of cells transitions to an elongated tube. The embryonic
284 sheath serves as a framework upon which the L1 cuticle is built [21,22,42]. The precuticle
285 components are endocytosed and recycled for subsequent rounds of cuticle synthesis.
286 Given the embryonic *mlt-11* promoter reporter expression we observed (Fig. 2C), we
287 imaged MLT-11::mNG in embryos from prior to elongation through to just prior to hatching
288 (Fig. 7A). Expression was detected in the posterior of bean stage embryos, quickly
289 encompassing the entire embryo by comma stage. MLT-11::mNG localizes to the aECM
290 of the animals and is endocytosed prior to hatching, similar to other precuticle
291 components [20].
292
293 Loss of other precuticle components causes embryonic lethality or morphogenesis
294 defects [20,23]. However, we had not observed embryonic defects with our promoter
295 element deletion strains, the *rol-9* allele, or our RNAi experiments. However, as RNAi
296 causes reduction-of-function, we turned to deletion alleles. MLT-11 is predicted to be a
297 large protein (234-341 kDA) with a signal sequence, a thyroglobulin domain, and 10
298 Kunitz protease inhibitor domains (Fig. 3A). Eight of the 10 Kunitz domains contain all 6
299 conserved cysteine residues that are necessary to form three disulfide bonds critical for
300 stabilizing the domain (Fig. S2)[58]. To prevent MLT-11 secretion, we deleted the signal
301 sequence. We also deleted the coding region downstream from the *rol-9(sc148)* indel,
302 removing Kunitz domains 3-10 (*mlt-11*Δ; Fig. 3A). We were unable to homozygose these
303 alleles, indicating embryonic lethality or sterility. As *mlt-11* is on the far right arm of
304 chromosome V in an area lacking classic genetic balancer chromosomes, we used a
305 *myo-2p::GFP::unc-54 3'UTR* insertion approximately 40 kb away to balance the deletions.
306 We never observed viable progeny from balanced mutant worms that lacked GFP in the
307 pharynx, but these balanced worms produced roughly 25% dead embryos, a rate
308 expected for a homozygous lethal mutation (Fig. 7B).

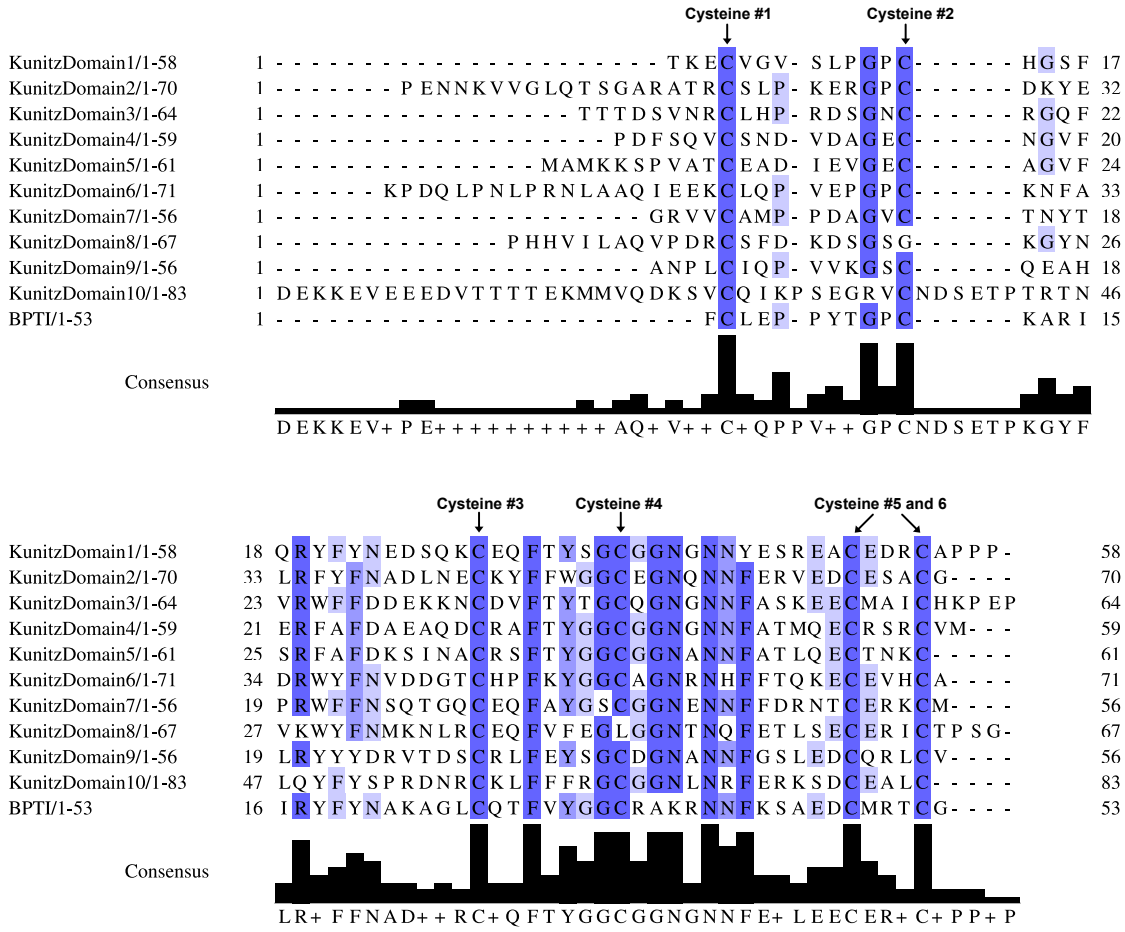

Supplemental Fig. 2. Alignment of MLT-11 homologs. MLT-11 homologs from the indicated nematode species were aligned using Clustal Omega. The length in amino acids of each homolog follows the species and homolog name. To the left and right of the alignment are amino acid positions of the end residues for each protein. Blue shading indicates conserved sequences and the histogram at the bottom depicts the degree of conservation with a consensus sequence listed below. The positions of the *C. elegans* MLT-11 signal sequence, thyroglobulin domain, and ten Kunitz domains are indicated. We note that we cut off the extended *P. pacificus* C-terminus (amino acids 2626-3742) since no sequence aligned to it as all proteins terminated at the *C. elegans* MLT-11 stop codon. No predicted motifs are found in the *P. pacificus* C-terminus.

We next examined the nature of the embryonic lethality in *mlt-11* deletion mutants using a DLG-1::mNG allele to mark adherens junctions [59]. In control embryos, DLG-1::mNG labeled adherens junctions in the pharynx, intestine, and hypodermis (Fig. 7C). Hypodermal cells stretched around the circumference of and down the length of the coiled embryo in relatively straight lines. In contrast, *mlt-11Δ* embryos matched to the same

315 stage displayed severe disorganization. The pharynx and foregut adherens junctions
316 appeared wild type, but the remainder of the junctions were disorganized and there was
317 evidence of invaginations in the hypodermis (Fig. 7C). These data implicate the signal
318 sequence and sequence within the Kunitz 3-10 region as being essential for hypodermal
319 organization during embryogenesis (Fig. 7C).
320
321 ***mlt-11(RNAi)* suppresses the blister phenotype of *bli-4* hypomorphic adults**
322 The expression timing of *mlt-11* and deletion phenotypes were reminiscent of the
323 precuticle components *noah-1* and *noah-2*, and the subtilisin/kexin family protease *bli-4*
324 [20,42]. *noah-1* and *noah-2* mutants are essential for embryonic integrity and elongation,
325 while *bli-4* null animals initially elongate but then retract and collapse [20,42]. We were
326 particularly intrigued by the similarity of MLT-11 to BLI-4 because both proteins are
327 expressed in larvae and embryos and essential for viability at both stages. MLT-11 is
328 endocytosed (Fig. 7A) while BLI-4 is ingested [42]. We hypothesized that MLT-11 could
329 conceivably inhibit BLI-4. In this model, a reduction in *bli-4* activity could be rescued by
330 reduction in *mlt-11* levels. *bli-4(e937)* is a hypomorphic allele that causes a blistered
331 cuticle in adult larvae (Fig. 8A)[43]. Strikingly, *mlt-11* completely suppressed the blistered
332 phenotype. To test whether *mlt-11* inactivation affected BLI-4 levels or localization, we
333 depleted *mlt-11* RNAi in a *bli-4::sfGFP* strain. There was no significant change in BLI-
334 4::sfGFP expression or localization in *mlt-11(RNAi)* compared to the control animals (Fig.
335 8B). These data indicate that reduction of MLT-11 levels compensates for reduction of
336 *bli-4* function.
337

338

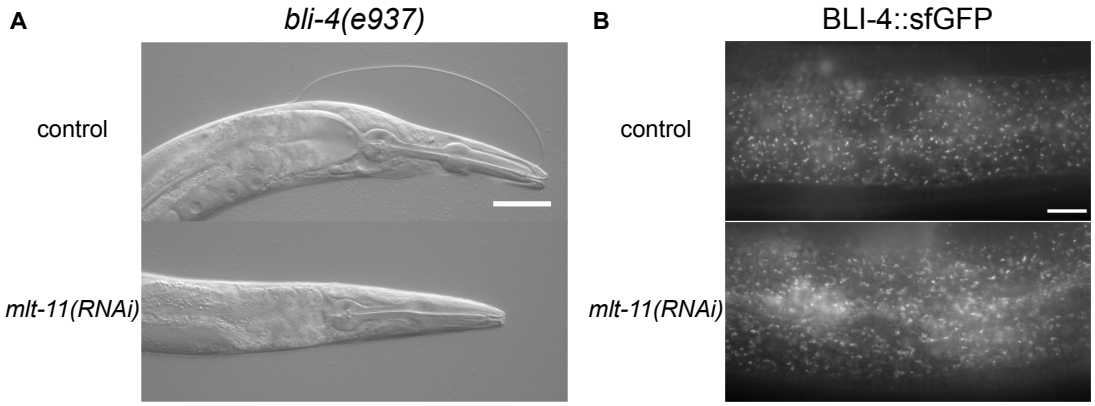

Fig. 8. *mlt-11(RNAi)* suppresses a reduction-of-function allele of *bli-4*. (A) Representative DIC images of *bli-4(e937)* adults grown on control or *mlt-11* RNAi plates. A large blister (separation of the cortical layer from the body of the worm) is indicated with an arrow. Over 200 animals were scored over two independent experiments. *bli-4(e937)* mutants displayed blistering in ~90% of adults similar to what Thacker *et al.* (1995) reported, which *mlt-11* RNAi completely suppressed the blister phenotype (B) Representative images of BLI-4::sfGFP seen in internal hypodermal punctae in control and *mlt-11(RNAi)* mid-late stage L4 larvae. Images are representative of >40 animals scored over two independent experiments. Scale bars are 20 µm.

339 **DISCUSSION**

340 Despite their importance, how aECMs are built and dynamically remodeled during
341 development and disease remains poorly understood. Using the *C. elegans* cuticle as a
342 model aECM we show that *mlt-11* is directly regulated by the NHR-23 transcription factor.
343 MLT-11::mNG transiently localizes to the embryonic and larval aECM before endocytosis
344 and trafficking to a compartment that is most likely lysosomal. MLT-11::mNG also lines
345 openings to the exterior (vulva, buccal cavity, excretory duct, rectal epithelium). *mlt-11*
346 inactivation affects the localization of translational fusions marking the basal (ROL-
347 6::mNG, COL-19), medial (BLI-1::mNG), and cortical layers (CUT-2) of the cuticle
348 indicating a broad role for MLT-11 in patterning this aECM. In agreement with these broad
349 defects in aECM component localization, *mlt-11* inactivation causes loss of the epithelial
350 barrier and activation of an epidermal damage reporter. Tissue-specific RNAi data
351 indicates that *mlt-11* may act primarily in seam cells, though a role in the hypodermis is
352 also supported. Alleles predicted to cause a loss of *mlt-11* function cause embryonic
353 lethality with severe disorganization of hypodermal adherens junctions. *mlt-11*

354 inactivation suppresses the blistering phenotype caused by the *e937* mutation in the *bli-*
355 *4* subtilisin/kexin family protease. Together, this work suggests that MLT-11 may be part
356 of the pre-cuticle and functions to coordinate proper assembly of the aECM.
357
358 ***mlt-11* is an NHR-23-regulated gene required for patterning of all cuticle layers**
359 *mlt-11* was identified as an *nhr-23*-regulated gene through studies using promoter
360 reporter and a microarray analysis of genes misregulated in L2 animals following *nhr-23*
361 RNAi [33,44]. NHR-23 ChIP-seq data identified four NHR-23 occupied regions 5' to the
362 transcription start site, and we showed that peaks 3 and 4 drive robust reporter expression
363 and NHR-23 controls the expression of a *mlt-11 peak 3* reporter. While it is not clear
364 whether NHR-23 regulates expression of these reporters through direct DNA binding or
365 whether the regulation is indirect, there are consensus sites that NHR-23 is known to bind
366 within or adjacent to these peak sequences (Fig. 2) [35]. Consistent with the reporter data,
367 deletion of the endogenous peak sequences revealed that peaks 3 and 4 produced the
368 strongest effect on MLT-11::mNG expression and a double deletion of peaks 3 and 4
369 results in even stronger reduction in expression. Despite robust hypodermal expression
370 and localization, our tissue-specific RNAi suggests that the seam cells are an important
371 site of *mlt-11* expression (Fig. 3,4,6). We consistently saw the most severe RNAi
372 phenotypes in tissue-specific RNAi strains using a seam cell enriched promoter and no
373 phenotypes from a hypodermal/intestinal-specific RNAi strain (Fig. 6)[32]. Consistent with
374 these data, we observed aberrant expression of ROL-6::mNG, CUT-2::mNG, and COL-
375 19::mNG over the seam cells (Fig. 4). We also see gaps in the alae following *mlt-11*
376 inactivation. Moreover, BLI-1 is normally excluded from the aECM over the seam cells
377 but invades this area following *mlt-11* knockdown (Fig. 4). These data were reminiscent
378 of our work on NHR-23 as depletion of this factor causes aberrant aECM formation over
379 the seam cells and *nhr-23* activity also was necessary in the seam cells for developmental
380 progression [32]. *nhr-23* and *lin-42* both regulate the molting timer and the heterochronic
381 pathway and these two timers need to be tightly coordinated [27–31,36]. Pharmacologic
382 uncoupling through nicotinic agonists results in animal death through rupturing when
383 animals molt before seam cell division is completed [60]. Exploring the tissue-specificity

384 and coordination of the molting and heterochronic timers and how the aECM might impact
385 these timers is an important future direction.
386
387 **A *mlt-11* allelic series**
388 Following *cis*-regulatory element deletion in the *mlt-11* promoter, deletion of *mlt-11* coding
389 sequence, and RNAi we observed a range of phenotypic severity: i) embryonic lethality;
390 ii) molting defects and developmental delay; iii) cuticle organization defects; and iv) cuticle
391 barrier defects. These mutants and *mlt-11(RNAi)* comprise an allelic series to link *mlt-11*
392 levels to specific phenotypes. Embryonic development seems to require the least MLT-
393 11 activity as we only encountered embryonic lethality when we prevented MLT-11
394 secretion through signal sequence deletion, or deleted the majority of the protein (Fig. 7).
395 Motility was also less sensitive to MLT-11 levels as we needed RNAi depletion to observe
396 phenotypes (Fig. S1). BLI-1 localization, developmental rate and the cuticle barrier
397 displayed intermediate sensitivity to MLT-11 levels as peak 3+4 deletion caused defects,
398 as did RNAi (Fig. 4, 5, 6). Finally ROL-6 organization seemed highly sensitive to MLT-11
399 levels, as peak 3 deletion caused a reduction of MLT-11 levels and aberrant ROL-6
400 localization especially over the seam cells (Fig. 4). MLT-11 has 10 predicted protease
401 inhibitor domains most of which contain residues necessary for Kunitz inhibitor activity
402 [58,61], which could buffer reduction of levels. It will be important to perform careful
403 structure-function analyses to determine the role of specific Kunitz domains and other
404 sequences in mediating this allelic series.
405
406 **Is MLT-11 a pre-cuticle component?**
407 The hallmarks of *bona fide* precuticle components are that they are secreted, transiently
408 localize in the aECM before being endocytosed and degraded in lysosomes [14–19].
409 Precuticle components are also found in the embryonic sheath and are required for
410 embryonic viability [20,23]. We found that MLT-11 is secreted and endocytosed in both
411 embryos and larvae (Fig. 3, 7). Predicted nulls or strong reduction-of-function alleles
412 cause embryonic death during elongation which is strikingly similar to *noah-1* and *noah-*
413 *2* mutants [20]. *mlt-11(RNAi)* animals display gaps in alae similar to precuticle mutants
414 [12], and we observed defective localization of mNG translational fusions marking each

415 layer of the adult cuticle (Fig. 4). If MLT-11 is indeed a precuticle component it would be
416 the first putative protease inhibitor to localize to this structure. What is MLT-11 doing in
417 this transient matrix? It could function as a protease inhibitor restraining protease
418 substrates until it is endocytosed, releasing the protease to digest aECM substrates.
419 Alternatively, MLT-11 could function as a scaffold to coordinate aECM and precuticle
420 assembly. The MLT-11 dynamics raise several questions. How is it endocytosed? It is
421 internalized in L4.7-L4.8 stage larvae while NOAH-1 is endocytosed in L4.9 larvae, so
422 there appears to be intriguing temporal regulation of endocytosis (Fig. 3) [32]. Additionally
423 MLT-11 localization in the aECM over the alae is lost in L4.6 stage larvae, earlier than
424 endocytosis from the hypodermal aECM. Understanding the mechanisms controlling
425 precuticle internalization will provide an important entry point into aECM dynamics during
426 development.
427
428 ***mlt-11* and *bli-4* genetically interact**
429 Our working model is that MLT-11 is a protease inhibitor that restrains the activity of
430 cognate protease(s). In looking for candidate substrates we looked for protease genes
431 that are essential and expressed in both embryos and larvae. While Kunitz domains are
432 typically serine protease inhibitors, in the flatworm *Fasciola hepatica* an atypical Kunitz
433 domain protein inhibits cysteine proteases, indicating a broader spectrum of potential
434 substrates [62]. BLI-4 was an intriguing candidate. Reduction-of-function alleles cause
435 either larval lethality or blistering, while nulls cause embryonic lethality but later in
436 development than *mlt-11* nulls (Fig. 7) [43,43,63]. *bli-4(0)* mutants complete elongation
437 but then the embryo retracts and loses organization [42]. BLI-4::sfGFP is secreted in
438 embryos and ingested rather than endocytosed. We reasoned that reducing *mlt-11*
439 activity might suppress *bli-4* hypomorphs by rebalancing protease activity, similar to how
440 inactivation of two antagonistic developmental regulators restores correct cell fates in the
441 *C. elegans* somatic gonad precursor cells [64]. When we inactivated *mlt-11* by RNAi we
442 completely suppressed the blister phenotype of *bli-4(e937)* hypomorphs. This effect was
443 not through regulating BLI-4 levels or localization as we saw no obvious changes in BLI-
444 4::sfGFP. These data could reflect a direct interaction between BLI-4 and MLT-11. In this
445 model, some *mlt-11* phenotypes could come from aberrant BLI-4 activity. Alternatively,

446 the interaction could be indirect with MLT-11 broadly affecting aECM organization. For
447 example, some suppressors of the *bli-1* blistered phenotype are collagen mutants that
448 are thought to make a more larval-like cuticle and eliminate the fluid-filled medial layer
449 [7]. Testing MLT-11 and BLI-4 for a direct interaction, exploring the nature of the
450 suppression, and testing for altered processing of predicted BLI-4 substrates are all
451 important future directions.
452

453 **Future perspective**

454 This work provides an entry point into understanding how a predicted protease inhibitor
455 regulates the structure and function of the *C. elegans* aECM. Going forward, it will be
456 critical to determine the biochemical activity of MLT-11 to determine what function(s) it
457 plays in the aECM before internalization and what its substrates are. As proteases are
458 important targets to combat parasitic nematode infections, understanding how they are
459 regulated during development by endogenous protease inhibitors will be critical to
460 develop novel approaches to combat this group of devastating pathogens.
461

462 **MATERIALS AND METHODS**

463 **Strains and culture**

464 *C. elegans* were cultured as originally described [65], except worms were grown on
465 MYOB media instead of NGM. MYOB agar was made as previously described [66].

466 **Strains created by injection in the Ward Lab and used in this study:**

Name	**Genotype**
JDW359	*ezIs2 III [fkh-6::GFP + unc-119(+)] ; him-8(e1489) IV ; F46B3.7(gk5359[loxP + myo-2p::GFP::unc-54 3' UTR + rps-27p::neoR::unc-54 3' UTR + loxP]) V.*
JDW371	*jsTi1493 {mosL loxP [wrdSi72(SCMp::pes-10delta::rde-1 CDS+3'UTR)] FRT3::mosR} IV ; rde-1(ne300) V [32]*

JDW380	*jsTi1493 {mosL loxP [wrdSi72(mlt-11(-2.8kb)p::mNeonGreen(dpi)::tbb-2 3'UTR)] FRT3::mosR} IV*
JDW387	*mlt-11(wrd82[mlt-11 Kunitz 3-10 deletion]) , oxTi633 [eft-3p::tdTomato::H2B::unc-54 3'UTR] / F46B3.7(gk5359[loxP + myo-2p::GFP::unc-54 3' UTR + rps-27p::neoR::unc-54 3' UTR + loxP]) V*
JDW389	*bli-1(wrd84[linker::mNeonGreen::3xFLAG::linker]) [32]*
JDW401	*mlt-11(wrd82[mlt-11 Kunitz 3-10 deletion]) , oxTi633 [eft-3p::tdTomato::H2B::unc-54 3'UTR] / F46B3.7(gk5359[loxP + myo-2p::GFP::unc-54 3' UTR + rps-27p::neoR::unc-54 3' UTR + loxP]) V. dlg-1(cp301[dlg-1::mNG-C1^3xFlag]) X*
JDW458	*rol-6(wrd117[rol-6::C-term mNeonGreen (dpi)::3xFLAG::linker]) [32]*
JDW510	*jsTi1493 {mosL loxP [wrdSi97(suro-1p::rde-1 CDS+3'UTR)] FRT3::mosR} IV ; rde-1 (ne300) V* (Johnson *et al.,* 2022) [32]
JDW511	*ezIs2 [fkh-6::GFP + unc-119(+)] / + III ; him-8(e1489) / + IV ; mlt-11(wrd126[mlt-11 signal sequence deletion...mNG::3xFLAG]) / F46B3.7(gk5359[loxP + myo-2p::GFP::unc-54 3' UTR + rps-27p::neoR::unc-54 3' UTR + loxP]) V*
JDW523	*mlt-11(wrd141[mlt-11 signal sequence deletion]) , oxTi633 [eft-3p::tdTomato::H2B::unc-54 3'UTR + Cbr-unc-119(+)] V*
JDW535	*jsSi1579 jsSi1706 jsSi1726 wrdSi103[loxP myo-2p::NLS::mNeonGreen, rps-0p HygR, loxP mlt-11p peak 3::pes-10 minimal promoter::mNeonGreen(dpi)::PEST::3xFLAG::tbb-2 3'UTR FRT3] II*
JDW541	*mlt-11(wrd153[mNG::3xFLAG internal]) V*
JDW551	*mlt-11(wrd158[mlt-11 promoter chip-seq peak 3 deletion]), oxTi633 [eft-3p::tdTomato::H2B::unc-54 3'UTR + Cbr-unc-119(+)] V*
JDW558	*mlt-11(wrd153[mNG::3xFLAG internal], wrd161[promoter chip-seq peak 2 deletion]) V*
JDW559	*mlt-11(wrd153[mNG::3xFLAG internal], wrd162[promoter chip-seq peak 3 deletion]) V*
JDW655	*cut-2(wrd233{cut-2::C-terminal modular linker::mNG::3xFLAG::linker]) V*

JDW663	*mlt-11(wrd153[mNG::3xFLAG internal], mlt-11(wrd237[mlt-11 promoter chip-seq peak 4 deletion]) V*
JDW666	*jsSi1579 jsSi1706 jsSi1726 wrdSi108[loxP myo-2p::NLS::mNeonGreen, rps-0p HygR, loxP mlt-11p peaks 1, 2 and 3::mNeonGreen(dpi)::tbb-2 3'UTR FRT3] II*
JDW667	*jsSi1579 jsSi1706 jsSi1726 wrdSi109[loxP myo-2p::NLS::mNeonGreen, rps-0p HygR, loxP mlt-11p peak 1::pes-10 minimal promoter::mNeonGreen(dpi)::tbb-2 3'UTR FRT3] II*
JDW668	*jsSi1579 jsSi1706 jsSi1726 wrdSi110[loxP myo-2p::NLS::mNeonGreen, rps-0p HygR, loxP mlt-11p peak 2::pes-10 minimal promoter::mNeonGreen(dpi)::tbb-2 3'UTR FRT3] II*
JDW669	*jsSi1579 jsSi1706 jsSi1726 wrdSi111[loxP myo-2p::NLS::mNeonGreen, rps-0p HygR, loxP mlt-11p peak 4::pes-10 minimal promoter::mNeonGreen(dpi)::tbb-2 3'UTR FRT3] II*
JDW670	*jsSi1579 jsSi1706 jsSi1726 wrdSi112[loxP myo-2p::NLS::mNeonGreen, rps-0p HygR, loxP mlt-11p enhancer 1::pes-10 minimal promoter::mNeonGreen(dpi)::tbb-2 3'UTR FRT3] II*
JDW671	*jsSi1579 jsSi1706 jsSi1726 wrdSi113[loxP myo-2p::NLS::mNeonGreen, rps-0p HygR, loxP mlt-11p enhancer 2::pes-10 minimal promoter::mNeonGreen(dpi)::tbb-2 3'UTR FRT3] II*
JDW687	*jsSi1579 jsSi1706 jsSi1726 wrdSi114[loxP myo-2p::NLS::mNeonGreen, rps-0p HygR, loxP mlt-11p(-5.2 kb)::mNeonGreen(dpi)::3xFLAG::PEST::tbb-2 3'UTR FRT3] II*
JDW696	*mlt-11(wrd153[mNG::3xFLAG internal], wrd268[mlt-11 promoter chip-seq peak 1 deletion]) V*
JDW703	*mlt-11(wrd153[mNG::3xFLAG internal], wrd162[promoter chip-seq peak 3 deletion]), wrd249[mlt-11 promoter chip-seq peak 4 deletion]) V*
JDW709	*mlt-11(wrd162[promoter chip-seq peak 3 deletion], wrd252[mlt-11 promoter chip-seq peak 4 deletion]) V*
JDW710	*rol-6(wrd253[rol-6::C-term mNeonGreen (dpi)::3xFLAG::linker]) II; mlt-11(wrd158[mlt-11 promoter chip-seq peak 3 deletion]) , oxTi633 [eft-3p::tdTomato::H2B::unc-54 3'UTR + Cbr-unc-119(+)] V*
JDW711	*jsSi1579 jsSi1706 jsSi1726 wrdSi115[loxP myo-2p::NLS::mNeonGreen, rps-0p HygR, loxP empty control::pes-10 minimal promoter::mNeonGreen(dpi)::tbb-2 3'UTR FRT3] II*

JDW713	*bli-1(wrd254[bli-1::internal mNeonGreen (dpi)::3xFLAG::linker]) II; mlt-11(wrd158[mlt-11 promoter chip-seq peak 3 deletion]) , oxTi633 [eft-3p::tdTomato::H2B::unc-54 3'UTR + Cbr-unc-119(+)] V*
JDW715	*rol-6(wrd255[rol-6::C-term mNeonGreen (dpi)::3xFLAG::linker]) II; mlt-11(wrd162[promoter chip-seq peak 3 deletion], wrd252[mlt-11 promoter chip-seq peak 4 deletion]) V*
JDW719	*jsSi1579 jsSi1706 jsSi1726 wrdSi116[loxP myo-2p::NLS::mNeonGreen, rps-0p HygR, loxP mlt-11p (Frand promoter -1977-5300 bp)::mNeonGreen (dpi)::3xFLAG::PEST::tbb-2 3'UTR FRT3] II*
JDW743	*bli-1(wrd254[bli-1::internal mNeonGreen (dpi)::3xFLAG::linker]) II; mlt-11(wrd158[mlt-11 promoter chip-seq peak 3 deletion]) , mlt-11(wrd288[mlt-11 promoter chip-seq peak 4 deletion]) , oxTi633 [eft-3p::tdTomato::H2B::unc-54 3'UTR + Cbr-unc-119(+)] V*
JDW750	*frIs7 [nlp-29p::GFP + col-12p::DsRed] IV ; mlt-11(wrd294[mlt-11 promoter chip-seq peak 3 deletion]) V*
JDW757	*frIs7 [nlp-29p::GFP + col-12p::DsRed] IV ; mlt-11(wrd294[mlt-11 promoter chip-seq peak 3 deletion] + wrd295[mlt-11 promoter chip-seq peak 4 deletion]) V*

467 **Strains provided by the *Caenorhabditis* Genetics Center:**

CB6193[67]	*bus-8B(e2885) X [55]*
CB937	*bli-4(e937) I [67]*
DZ325	*ezIs2 III [fkh-6::GFP + unc-119(+)] ; him-8(e1489) IV* [68]
EG7968	*unc-119(ed3) III; oxTi633 [eft-3p::tdTomato::H2B::unc-54 3'UTR + Cbr-unc-119(+)] V [69]*
JU2039	*mfIs70 [lin-31p::rde-1 + myo2p::GFP] IV ; rde-1(ne219) V [70]*
LP598	*dlg-1(cp301[dlg-1::mNG-C1^3xFlag]) X [59]*
MGH171	*alxIs9 [vha-6p::sid-1::SL2::GFP] sid-1(qt9) V ; alxIs9 [71]*
N2	*Wild-type[56]*
IG274	*frIs7 [nlp-29p::GFP + col-12p::DsRed] IV*

QK52	*rde-1(ne219) V ; xkIs99(wrt-2p::rde-1::unc-54 3'UTR) [71]*
VC4276	*F46B3.7(gk5359[loxP + myo-2p::GFP::unc-54 3' UTR + rps-27p::neoR::unc-54 3' UTR + loxP]) V* [72]
VP303	*rde-1(ne219) V ; kbIs7[nhx-2p::rde-1 + rol-6(su1006)]) [73]*
WM118	*rde-1(ne300) V ; neIs9(neIs9 [myo-3::HA::RDE-1 + rol-6(su1006)]) X [74]*
NM5548	*jsSi1579 jsSi1706 jsSi1726[loxP myo-2p FRT nlsCyOFP myo-2 3' mex-5p FLP D5 glh-2 3' FRT3] II [75]*

468

469 **Other strains**

470 PHX4625 *col-19::mNG(cyb4625) X* was a gift from Dr. Andrew Chisholm and will be
471 described elsewhere. ARF403 *aaaIs24[egl-18p::utrnch::gfp::unc-54 3'UTR, ttx-3::gfp]*
472 was previously published and a gift from Ali Frand and Meera Sundaram [12].

473

474 **Genome Editing**

475 All plasmids used are listed in Table S1. Annotated plasmid sequence files are provided
476 in File S1. Specific cloning details and primers used are available upon request. JDW380
477 *jsTi1493 {mosL loxP [wrdSi72(mlt-11(-2.8kb)p::mNeonGreen(dpi)::tbb-2 3'UTR)]*
478 *FRT3::mosR} IV* was created by recombination-mediated cassette exchange
479 (RMCE)[76]. A 2.8 kb *mlt-11* promoter fragment was initially Gibson cloned into the
480 *NLS::mScarlet (dpi)::tbb-2 3'UTR* vector pJW1841 [77] to generate pJW1934. The
481 mScarlet cassette was then replaced with mNeonGreen (dpi) to generate pJW2229. The
482 *mlt-11p (-2.8kb) mNeonGreen (dpi)-tbb-2 3'UTR* fragment was PCR amplified from
483 pJW2229 and Gibson cloned into *Sph*I-HF+*Spe*I-HF double digested RMCE integration
484 vector pLF3FShC to produce pJW2337. This vector was integrated into NM5179 and the
485 SEC was excised as previously described [76].

486

487 A pJW2361 *mNeonGreen(dpi)::3xFLAG::PEST-tbb-2 3'UTR* vector for SapTrap with ATG
488 and GTA connectors was constructed by linearizing pJW2322 [48] by PCR and Gibson
489 cloning in PCR amplified *mNeonGreen (dpi)::3xFLAG* from pJW2172 and a

490 *linker::PEST::tbb-2 3'UTR* from pJW1836 [77]. The pJW2286 *mlt-11p (-2.8 kb)* promoter
491 for SapTrap cloning was previously described [48]. The *mlt-11* promoter fragment from
492 Frand *et al.* (2005) and the *mlt-11p (-5.3 kb)* promoter fragment were PCR amplified from
493 a fosmid containing the *mlt-11* gene and Gibson cloned into linearized pJW2286 to make
494 pJW2451 and pJW2457, respectively. These *mlt-11* promoter plasmids were SapTrap
495 cloned with pJW2361 and pNM4216 to generate insertion vectors for rRMCE [75,78]. The
496 remaining promoter reporters were constructed by SapTrap cloning and rapid RMCE
497 [75,78]. A pJW2365 *pes-10 minimal promoter::mNeonGreen(dpi):: 3xFLAG::PEST-tbb-2*
498 *3'UTR* vector for SapTrap with ATG and GTA connectors was constructed by linearing
499 pJW2361 and Gibson cloning in a *pes-10* minimal promoter amplified from pJW1947 [77].
500 The ATAC-seq and NHR-23 ChIP-seq peak DNA sequences were PCR amplified from
501 pJW2337 and Gibson cloned into pDONR221 with TGG and ATG connectors for
502 SapTrap. These plasmids were then SapTrap cloned with pJW2365 and pNM4216 to
503 generate insertion vectors for rRMCE [75,78].
504
505 *mlt-11* promoter and coding region deletion strains were created by injection of Cas9
506 ribonucleoprotein complexes (RNPs)[79,80] [700 ng/µl IDT Cas9, 115 ng/µl each crRNA
507 and 250 ng/µl IDT tracrRNA], oligonucleotide repair template (110 ng/µl) and pSEM229
508 co-injection marker (25 ng/µl)[81] for screening into strain EG7968. Where possible, we
509 selected "GGNGG" crRNA targets as these have been the most robust in our hand and
510 support efficient editing [82]. F1s expressing the co-injection marker were isolated to lay
511 eggs and screened by PCR for the deletion. For lethal mutations, F2 progeny of a verified
512 F1 deletion mutant were crossed to JDW359 males expressing *myo-2::GFP* to genetically
513 balance the mutation. Genotyping primers are provided in Table S2. JDW389 was created
514 by injection of RNPs [700 ng/µl IDT Cas9, 115 ng/µl crRNA and 250 ng/µl IDT tracrRNA]
515 and a dsDNA repair template (25-50 ng/ul) created by PCR amplification of a plasmid
516 template into N2 animals [79,80](Table S1). PCR products were melted to boost editing
517 efficiency, as previously described [83]. For the *mlt-11* internal knock-in, the
518 mNeonGreen::3xFLAG cassette was inserted in an unstructured region of exon 7. The
519 JDW655 *cut-2*::mNG::3xFLAG knock-in used a pJW2332 repair template, which will be
520 described elsewhere (J.M.R. and J.D.W., unpublished). Sequences of CRISPR/Cas9-

521 mediated genome edits are provided in File S2. crRNAs used are provided in Table S3
522 and repair template oligos for deletions are provided in Table S4. F1 progeny were
523 screened by mNeonGreen expression.
524
525 **Imaging**
526 Synchronized animals were collected from MYOB, control, or auxin plates by either
527 picking or washing off plates. For washing, 1000 µl of M9 + 2% gelatin was added to the
528 plate or well, agitated to suspend animals in M9+gelatin, and then transferred to a 1.5 ml
529 tube. Animals were spun at 700xg for 1 min. The media was then aspirated off and
530 animals were resuspended in 500µl M9 + 2% gelatin with 5 mM levamisole. 12 µl of
531 animals in M9 +gel with levamisole solution were placed on slides with a 2% agarose pad
532 and secured with a coverslip. For picking, animals were transferred to a 10 µl drop of
533 M9+5 mM levamisole on a 2% agarose pad on a slide and secured with a coverslip.
534 Synchronized embryos were picked to a 2% agarose pad on a slide, secured with a
535 sealed coverslip and imaged once an hour. Heterozygous Kunitz 3-10Δ embryos were
536 identified by initial expression of a pharyngeal myo-2p::GFP::unc-54 3'UTR reporter on
537 the balancing wildtype chromosome. Images were acquired using a Plan-Apochromat
538 40x/1.3 Oil DIC lens or a Plan-Apochromat 63x/1.4 Oil DIC lens on an AxioImager M2
539 microscope (Carl Zeiss Microscopy, LLC) equipped with a Colibri 7 LED light source and
540 an Axiocam 506 mono camera. Acquired images were processed through Fiji software
541 (version: 2.0.0- rc-69/1.52p). For direct comparisons within a figure, we set the exposure
542 conditions to avoid pixel saturation of the brightest sample and kept equivalent exposure
543 for imaging of the other samples.
544
545 For the embryo imaging timecourse (Fg. 7A), 15-20 mlt-11(wrd153[mNG::3xFLAG
546 internal]) gravid adults were plated on a 6 cm plate seeded with OP50 and allowed to lay
547 eggs for ~3 hours. Adults were removed and embryos were collected with an eyelash pick
548 for imaging. A microscope slide was coated with a 1 mm thick agarose pad made with
549 2% agarose in milli-Q water. Embryos were transferred to the agarose pad and coated
550 with 15 uL of an M9+gelatin solution. A coverslip was added and the edges were sealed
551 with nail polish to prevent liquid evaporation. Slides were imaged at 100x magnification

552 on the above described Zeiss Axioimager. Embryo positions were marked via the 'Tiles'
553 feature and snaps were taken of each embryo every 15 minutes for 4 hours or until the
554 slide began to appear dry. Exposure times were kept constant throughout the timecourse.
555 Embryo stages imaged ranged from ~100 cell stage to 3-fold, with at least 10 embryos
556 observed for each stage across three replicate experiments.
557
558 **RNAi Knockdown**
559 RNA interference experiments were performed as in Johnson *et al.* (2023). Control RNAi
560 used an empty L4440. The *mlt-11 (RNAi)* vector was streaked from the Ahringer library
561 [84]. Vector sequences are provided in File S1.
562
563 **Hoechst staining**
564 Hoechst 33258 staining was performed as described previously [85], except that we used
565 10 µg/ml of Hoechst 33258 as previously described [86]. Two biological replicates were
566 performed examining 50 animals per experiment. Representative images were taken with
567 equivalent exposures using a 63× Oil DIC lens, as described in the imaging section.
568
569 **Acknowledgements**
570 We would like to thank Prof. David Fay and John C. Clancy for helpful conversations. We
571 thank Krista Myles, Patricia Bliatout, Zoe Johnson, Javier Hernandez Lopez, Zoie Reyna,
572 Emma Cadena, Valarie Hallin, and Olivia Vedar for research support. We thank Prof. Ali
573 Frand and Prof. Michael Nonet for strains and Prof. Meera Sundaram and Prof. Andrew
574 Chisholm for strains and helpful discussion. Some strains were provided by the
575 *Caenorhabditis* Genetics Center, which is funded by the NIH Office of Research
576 Infrastructure Programs [P40 OD010440].
577
578 **Competing interests**
579 The authors declare no competing or financial interests.
580
581 **Author Contributions**
582 Conceptualization: J.M.R., J.D.W., M.T.L.

583 Methodology: J.M.R., A.T., M.T.L., K.J., A.J., A.A.V., V.T.P., J.D.W.
584 Validation: J.M.R., A.T., M.T.L., K.J., A.J., A.A.V., V.T.P., J.D.W.
585 Formal analysis:J.M.R., A.T., M.T.L., K.J., A.J., A.A.V., V.T.P., J.D.W.
586 Resources: J.M.R., J.D.W.
587 Data curation: J.M.R., J.D.W.
588 Writing - original draft: J.M.R., J.D.W.
589 Writing - review & editing: J.M.R., A.T., M.T.L., K.J., A.J., A.A.V., V.P., J.D.W.
590 Supervision: J.M.R., J.D.W.
591 Project administration: J.D.W.
592 Funding acquisition: J.D.W.
593

594 **Funding**
595 This work was funded by the National Institutes of Health (NIH) National Institute
596 of General Medical Sciences (NIGMS) [R00GM107345 and R01 GM138701] to J.D.W.
597

598 **REFERENCES**

599 1. Li Zheng S, Adams JG, Chisholm AD. Form and function of the apical extracellular matrix:
600 new insights from *Caenorhabditis elegans, Drosophila melanogaster*, and the vertebrate
601 inner ear. Fac Rev. 2020;9: 27. doi:10.12703/r/9-27
602 2. Diller RB, Tabor AJ. The Role of the Extracellular Matrix (ECM) in Wound Healing: A
603 Review. Biomimetics. 2022;7: 87. doi:10.3390/biomimetics7030087
604 3. Bonnans C, Chou J, Werb Z. Remodelling the extracellular matrix in development and
605 disease. Nat Rev Mol Cell Biol. 2014;15: 786–801. doi:10.1038/nrm3904
606 4. Page AP, Johnstone IL. The cuticle. WormBook Online Rev C Elegans Biol. 2007; 1–15.
607 doi:10.1895/wormbook.1.138.1
608 5. Edgar RS, Cox GN, Kusch M, Politz JC. The Cuticle of *Caenorhabditis elegans*. J Nematol.
609 1982;14: 248–258.
610 6. Cox GN, Kusch M, Edgar RS. Cuticle of *Caenorhabditis elegans*: its isolation and partial
611 characterization. J Cell Biol. 1981;90: 7–17. doi:10.1083/jcb.90.1.7
612 7. Adams JRG, Pooranachithra M, Jyo EM, Zheng SL, Goncharov A, Crew JR, et al.
613 Nanoscale patterning of collagens in *C. elegans* apical extracellular matrix. Nat Commun.
614 2023;14: 7506. doi:10.1038/s41467-023-43058-9
615 8. Ristoratore F, Cermola M, Nola M, Bazzicalupo P, Favre R. Ultrastructural immuno-

616 localization of CUT-1 and CUT-2 antigenic sites in the cuticles of the nematode
617 *Caenorhabditis elegans*. J Submicrosc Cytol Pathol. 1994;26: 437–443.
618 9. Peixoto CA, De Souza W. Freeze-fracture and deep-etched view of the cuticle of
619 *Caenorhabditis elegans*. Tissue Cell. 1995;27: 561–568. doi:10.1016/s0040-
620 8166(05)80065-5
621 10. Blaxter ML. Cuticle surface proteins of wild type and mutant *Caenorhabditis elegans*. J Biol
622 Chem. 1993;268: 6600–6609.
623 11. Bada Juarez J, O'Rourke D, Judge P, Liu L, Hodgkin J, Watts A. Lipodisqs for eukaryote
624 lipidomics with retention of viability: Sensitivity and resistance to Leucobacter infection
625 linked to C.elegans cuticle composition. Chem Phys Lipids. 2019;222. Available:
626 https://ora.ox.ac.uk/objects/uuid:4d3c3aa1-3f12-443c-8ef0-c3647759832c
627 12. Katz SS, Barker TJ, Maul-Newby HM, Sparacio AP, Nguyen KCQ, Maybrun CL, et al. A
628 transient apical extracellular matrix relays cytoskeletal patterns to shape permanent
629 acellular ridges on the surface of adult *C. elegans*. PLOS Genet. 2022;18: e1010348.
630 doi:10.1371/journal.pgen.1010348
631 13. Lažetić V, Fay DS. Molting in *C. elegans*. Worm. 2017;6: 1–20.
632 doi:10.1080/21624054.2017.1330246
633 14. Cohen JD, Sundaram MV. *C. elegans* Apical Extracellular Matrices Shape Epithelia. J Dev
634 Biol. 2020;8: 23. doi:10.3390/jdb8040023
635 15. Cohen JD, Flatt KM, Schroeder NE, Sundaram MV. Epithelial Shaping by Diverse Apical
636 Extracellular Matrices Requires the Nidogen Domain Protein DEX-1 in *Caenorhabditis*
637 *elegans*. Genetics. 2019;211: 185–200. doi:10.1534/genetics.118.301752
638 16. Gill HK, Cohen JD, Ayala-Figueroa J, Forman-Rubinsky R, Poggioli C, Bickard K, et al.
639 Integrity of Narrow Epithelial Tubes in the C. elegans Excretory System Requires a
640 Transient Luminal Matrix. PLoS Genet. 2016;12: e1006205.
641 doi:10.1371/journal.pgen.1006205
642 17. Flatt KM, Beshers C, Unal C, Cohen JD, Sundaram MV, Schroeder NE. Epidermal
643 Remodeling in *Caenorhabditis elegans* Dauers Requires the Nidogen Domain Protein
644 DEX-1. Genetics. 2019;211: 169–183. doi:10.1534/genetics.118.301557
645 18. Forman-Rubinsky R, Cohen JD, Sundaram MV. Lipocalins Are Required for Apical
646 Extracellular Matrix Organization and Remodeling in Caenorhabditis elegans. Genetics.
647 2017;207: 625–642. doi:10.1534/genetics.117.300207
648 19. Serra ND, Sundaram MV. Transcytosis in the development and morphogenesis of
649 epithelial tissues. EMBO J. 2021;n/a: e106163. doi:10.15252/embj.2020106163

650 20. Vuong-Brender TTK, Suman SK, Labouesse M. The apical ECM preserves embryonic
651 integrity and distributes mechanical stress during morphogenesis. Development. 2017;144:
652 4336–4349. doi:10.1242/dev.150383
653 21. Priess JR, Hirsh DI. *Caenorhabditis elegans* morphogenesis: The role of the cytoskeleton
654 in elongation of the embryo. Developmental Biology. 1986. pp. 156–173.
655 22. Costa M, Draper BW, Priess JR. The role of actin filaments in patterning the
656 *Caenorhabditis elegans* cuticle. Dev Biol. 1997;184: 373–384. doi:10.1006/dbio.1997.8530
657 23. Kelley M, Yochem J, Krieg M, Calixto A, Heiman MG, Kuzmanov A, et al. FBN-1, a fibrillin-
658 related protein, is required for resistance of the epidermis to mechanical deformation
659 during *C. elegans* embryogenesis. eLife. 2015;4: 1629. doi:10.7554/eLife.06565
660 24. Cohen JD, Sparacio AP, Belfi AC, Forman-Rubinsky R, Hall DH, Maul-Newby H, et al. A
661 multi-layered and dynamic apical extracellular matrix shapes the vulva lumen in
662 *Caenorhabditis elegans*. Shen K, Sengupta P, Sherwood DR, editors. eLife. 2020;9:
663 e57874. doi:10.7554/eLife.57874
664 25. Hendriks G-J, Gaidatzis D, Aeschimann F, Großhans H. Extensive oscillatory gene
665 expression during *C. elegans* larval development. Mol Cell. 2014;53: 380–392.
666 doi:10.1016/j.molcel.2013.12.013
667 26. Meeuse MW, Hauser YP, Morales Moya LJ, Hendriks G, Eglinger J, Bogaarts G, et al.
668 Developmental function and state transitions of a gene expression oscillator in
669 *Caenorhabditis elegans*. Mol Syst Biol. 2020;16: e9975. doi:10.15252/msb.20209498
670 27. Jeon M, Gardner HF, Miller EA, Deshler J, Rougvie AE. Similarity of the *C. elegans*
671 Developmental Timing Protein LIN-42 to Circadian Rhythm Proteins. Science. 1999;286:
672 1141–1146. doi:10.1126/science.286.5442.1141
673 28. Tennessen JM, Gardner HF, Volk ML, Rougvie AE. Novel heterochronic functions of the
674 *Caenorhabditis elegans* period-related protein LIN-42. Dev Biol. 2006;289: 30–43.
675 doi:10.1016/j.ydbio.2005.09.044
676 29. Monsalve GC, Van Buskirk C, Frand AR. LIN-42/PERIOD controls cyclical and
677 developmental progression of *C. elegans* molts. Curr Biol CB. 2011;21: 2033–2045.
678 doi:10.1016/j.cub.2011.10.054
679 30. Spangler RK, Ashley GE, Braun K, Wruck D, Ramos-Coronado A, Ragle JM, et al. A
680 conserved chronobiological complex times *C. elegans* development. bioRxiv; 2024. p.
681 2024.05.09.593322. doi:10.1101/2024.05.09.593322
682 31. Hayes GD, Frand AR, Ruvkun G. The *mir-84* and *let-7* paralogous microRNA genes of
683 *Caenorhabditis elegans* direct the cessation of molting via the conserved nuclear hormone

684 receptors NHR-23 and NHR-25. Dev Camb Engl. 2006;133: 4631–4641.
685 doi:10.1242/dev.02655
686 32. Johnson LC, Vo AA, Clancy JC, Myles KM, Pooranachithra M, Aguilera J, et al. NHR-23
687 activity is necessary for *C. elegans* developmental progression and apical extracellular
688 matrix structure and function. Dev Camb Engl. 2023;150: dev201085.
689 doi:10.1242/dev.201085
690 33. Kouns NA, Nakielna J, Behensky F, Krause MW, Kostrouch Z, Kostrouchova M. NHR-23
691 dependent collagen and hedgehog-related genes required for molting. Biochem Biophys
692 Res Commun. 2011;413: 515–520. doi:10.1016/j.bbrc.2011.08.124
693 34. Kostrouchova M, Krause M, Kostrouch Z, Rall JE. Nuclear hormone receptor CHR3 is a
694 critical regulator of all four larval molts of the nematode *Caenorhabditis elegans*. Proc Natl
695 Acad Sci U S A. 2001;98: 7360–7365. doi:10.1073/pnas.131171898
696 35. Kostrouchova M, Krause M, Kostrouch Z, Rall JE. CHR3: a *Caenorhabditis elegans*
697 orphan nuclear hormone receptor required for proper epidermal development and molting.
698 Development. 1998;125: 1617–1626.
699 36. Patel R, Galagali H, Kim JK, Frand AR. Feedback between a retinoid-related nuclear
700 receptor and the *let-7* microRNAs controls the pace and number of molting cycles in *C.*
701 *elegans*. eLife. 2022;11: e80010. doi:10.7554/eLife.80010
702 37. Davis MW, Birnie AJ, Chan AC, Page AP, Jorgensen EM. A conserved metalloprotease
703 mediates ecdysis in *Caenorhabditis elegans*. Development. 2004;131: 6001–6008.
704 doi:10.1242/dev.01454
705 38. Hashmi S, Zhang J, Oksov Y, Lustigman S. The *Caenorhabditis elegans* cathepsin Z-like
706 cysteine protease, Ce-CPZ-1, has a multifunctional role during the worms' development. J
707 Biol Chem. 2004;279: 6035–6045. doi:10.1074/jbc.M312346200
708 39. Kim TH, Kim YJ, Cho JW, Shim J. A novel zinc-carboxypeptidase SURO-1 regulates
709 cuticle formation and body morphogenesis in *Caenorhabditis elegans*. FEBS Lett.
710 2011;585: 121–127. doi:10.1016/j.febslet.2010.11.020
711 40. Stepek G, McCormack G, Birnie AJ, Page AP. The astacin metalloprotease moulting
712 enzyme NAS-36 is required for normal cuticle ecdysis in free-living and parasitic
713 nematodes. Parasitology. 2011;138: 237–248. doi:10.1017/S0031182010001113
714 41. Stepek G, McCormack G, Page AP. Collagen processing and cuticle formation is catalysed
715 by the astacin metalloprotease DPY-31 in free-living and parasitic nematodes. Int J
716 Parasitol. 2010;40: 533–542. doi:10.1016/j.ijpara.2009.10.007
717 42. Birnbaum SK, Cohen JD, Belfi A, Murray JI, Adams JRG, Chisholm AD, et al. The

718 proprotein convertase BLI-4 promotes collagen secretion prior to assembly of the
719 *Caenorhabditis elegans* cuticle. PLOS Genet. 2023;19: e1010944.
720 doi:10.1371/journal.pgen.1010944
721 43. Thacker C, Peters K, Srayko M, Rose AM. The *bli-4* locus of *Caenorhabditis elegans*
722 encodes structurally distinct kex2/subtilisin-like endoproteases essential for early
723 development and adult morphology. Genes Dev. 1995;9: 956–971.
724 doi:10.1101/gad.9.8.956
725 44. Frand AR, Russel S, Ruvkun G. Functional Genomic Analysis of *C. elegans* Molting. PLoS
726 Biol. 2005;3: e312. doi:10.1371/journal.pbio.0030312
727 45. Stepek G, McCormack G, Page AP. The kunitz domain protein BLI-5 plays a functionally
728 conserved role in cuticle formation in a diverse range of nematodes. Mol Biochem
729 Parasitol. 2010;169: 1–11. doi:10.1016/j.molbiopara.2009.08.005
730 46. Gerstein MB, Lu ZJ, Van Nostrand EL, Cheng C, Arshinoff BI, Liu T, et al. Integrative
731 Analysis of the *Caenorhabditis elegans* Genome by the modENCODE Project. Sci N Y NY.
732 2010;330: 1775–1787. doi:10.1126/science.1196914
733 47. Mok DZL, Sternberg PW, Inoue T. Morphologically defined sub-stages of *C. elegans* vulval
734 development in the fourth larval stage. BMC Dev Biol. 2015; 1–8. doi:10.1186/s12861-015-
735 0076-7
736 48. Clancy JC, Vo AA, Myles KM, Levenson MT, Ragle JM, Ward JD. Experimental
737 considerations for study of *C. elegans* lysosomal proteins. G3 GenesGenomesGenetics.
738 2023; jkad032. doi:10.1093/g3journal/jkad032
739 49. Peixoto CA, de Melo JV, Kramer JM, de Souza W. Ultrastructural Analyses of the
740 *Caenorhabditis elegans rol-6 (su1006)* Mutant, Which Produces Abnormal Cuticle
741 Collagen. J Parasitol. 1998;84: 45–49. doi:10.2307/3284528
742 50. Kim TH, Kim DH, Nam HW, Park SY, Shim J, Cho JW. Tyrosylprotein sulfotransferase
743 regulates collagen secretion in *Caenorhabditis elegans*. Mol Cells. 2010;29: 413–418.
744 doi:10.1007/s10059-010-0049-4
745 51. Thein MC, McCormack G, Winter AD, Johnstone IL, Shoemaker CB, Page AP.
746 *Caenorhabditis elegans* exoskeleton collagen COL-19: an adult-specific marker for
747 collagen modification and assembly, and the analysis of organismal morphology. Dev Dyn
748 Off Publ Am Assoc Anat. 2003;226: 523–539. doi:10.1002/dvdy.10259
749 52. Tong A, Lynn G, Ngo V, Wong D, Moseley SL, Ewbank JJ, et al. Negative regulation of
750 *Caenorhabditis elegans* epidermal damage responses by death-associated protein kinase.
751 Proc Natl Acad Sci U S A. 2009;106: 1457–1461. doi:10.1073/pnas.0809339106

752 53. Lassandro F, Sebastiano M, Zei F, Bazzicalupo P. The role of dityrosine formation in the
753 crosslinking of CUT-2, the product of a second cuticlin gene of *Caenorhabditis elegans*.
754 Mol Biochem Parasitol. 1994;65: 147–159. doi:10.1016/0166-6851(94)90123-6
755 54. Cox GN, Staprans S, Edgar RS. The cuticle of *Caenorhabditis elegans*: II. Stage-specific
756 changes in ultrastructure and protein composition during postembryonic development. Dev
757 Biol. 1981;86: 456–470. doi:10.1016/0012-1606(81)90204-9
758 55. Partridge FA, Tearle AW, Gravato-Nobre MJ, Schafer WR, Hodgkin J. The *C. elegans*
759 glycosyltransferase BUS-8 has two distinct and essential roles in epidermal
760 morphogenesis. Dev Biol. 2008;317: 549–559. doi:10.1016/j.ydbio.2008.02.060
761 56. Pujol N, Cypowyj S, Ziegler K, Millet A, Astrain A, Goncharov A, et al. Distinct innate
762 immune responses to infection and wounding in the *C. elegans* epidermis. Curr Biol.
763 2008;18: 481–489. doi:10.1016/j.cub.2008.02.079
764 57. Zugasti O, Ewbank JJ. Neuroimmune regulation of antimicrobial peptide expression by a
765 noncanonical TGF-β signaling pathway in *Caenorhabditis elegans* epidermis. Nat
766 Immunol. 2009;10: 249–256. doi:10.1038/ni.1700
767 58. Ranasinghe S, McManus DP. Structure and function of invertebrate Kunitz serine protease
768 inhibitors. Dev Comp Immunol. 2013;39: 219–227. doi:10.1016/j.dci.2012.10.005
769 59. Heppert JK, Pani AM, Roberts AM, Dickinson DJ, Goldstein B. A CRISPR Tagging-Based
770 Screen Reveals Localized Players in Wnt-Directed Asymmetric Cell Division. Genetics.
771 2018;208: 1147–1164. doi:10.1534/genetics.117.300487
772 60. Ruaud A-F, Bessereau J-L. Activation of nicotinic receptors uncouples a developmental
773 timer from the molting timer in *C. elegans*. Development. 2006;133: 2211–2222.
774 doi:10.1242/dev.02392
775 61. Ascenzi P, Bocedi A, Bolognesi M, Spallarossa A, Coletta M, Cristofaro R, et al. The
776 Bovine Basic Pancreatic Trypsin Inhibitor (Kunitz Inhibitor): A Milestone Protein. Curr
777 Protein Pept Sci. 2003;4: 231–251. doi:10.2174/1389203033487180
778 62. Smith D, Cwiklinski K, Jewhurst H, Tikhonova IG, Dalton JP. An atypical and functionally
779 diverse family of Kunitz-type cysteine/serine proteinase inhibitors secreted by the helminth
780 parasite *Fasciola hepatica*. Sci Rep. 2020;10: 20657. doi:10.1038/s41598-020-77687-7
781 63. Thacker C, Srayko M, Rose AM. Mutational analysis of bli-4/kpc-4 reveals critical residues
782 required for proprotein convertase function in C. elegans. Gene. 2000;252: 15–25.
783 doi:10.1016/s0378-1119(00)00211-0
784 64. Asahina M, Valenta T, Silhánková M, Korinek V, Jindra M. Crosstalk between a nuclear
785 receptor and beta-catenin signaling decides cell fates in the *C. elegans* somatic gonad.

786 Dev Cell. 2006;11: 203–211. doi:10.1016/j.devcel.2006.06.003
787 65. Brenner S. The genetics of *Caenorhabditis elegans*. Genetics. 1974;77: 71–94.
788 66. Church DL, Guan KL, Lambie EJ. Three genes of the MAP kinase cascade, *mek-2*, *mpk-*
789 *1/sur-1* and *let-60 ras*, are required for meiotic cell cycle progression in *Caenorhabditis*
790 *elegans*. Development. 1995;121: 2525–2535.
791 67. Peters K, McDowall J, Rose AM. Mutations in the *bli-4* (I) locus of *Caenorhabditis elegans*
792 disrupt both adult cuticle and early larval development. Genetics. 1991;129: 95–102.
793 doi:10.1093/genetics/129.1.95
794 68. Chang W, Tilmann C, Thoemke K, Markussen F-H, Mathies LD, Kimble J, et al. A forkhead
795 protein controls sexual identity of the *C. elegans* male somatic gonad. Development.
796 2004;131: 1425–1436. doi:10.1242/dev.01012
797 69. Frøkjær-Jensen C, Davis MW, Sarov M, Taylor J, Flibotte S, LaBella M, et al. Random and
798 targeted transgene insertion in *Caenorhabditis elegans* using a modified *Mos1* transposon.
799 Nat Methods. 2014;11: 529–534. doi:10.1038/nmeth.2889
800 70. Barkoulas M, van Zon JS, Milloz J, Van Oudenaarden A, Félix M-A. Robustness and
801 Epistasis in the *C. elegans* Vulval Signaling Network Revealed by Pathway Dosage
802 Modulation. Dev Cell. 2013;24: 64–75. doi:10.1016/j.devcel.2012.12.001
803 71. Melo JA, Ruvkun G. Inactivation of conserved *C. elegans* genes engages pathogen- and
804 xenobiotic-associated defenses. Cell. 2012;149: 452–466. doi:10.1016/j.cell.2012.02.050
805 72. Au V, Li-Leger E, Raymant G, Flibotte S, Chen G, Martin K, et al. CRISPR/Cas9
806 Methodology for the Generation of Knockout Deletions in *Caenorhabditis elegans*. G3.
807 2019;9: 135–144. doi:10.1534/g3.118.200778
808 73. Espelt MV, Estevez AY, Yin X, Strange K. Oscillatory Ca2+ signaling in the isolated
809 *Caenorhabditis elegans* intestine: role of the inositol-1,4,5-trisphosphate receptor and
810 phospholipases C beta and gamma. J Gen Physiol. 2005;126: 379–392.
811 doi:10.1085/jgp.200509355
812 74. Watts JS, Harrison HF, Omi S, Guenthers Q, Dalelio J, Pujol N, et al. New Strains for
813 Tissue-Specific RNAi Studies in *Caenorhabditis elegans*. G3. 2020;10: 4167–4176.
814 doi:10.1534/g3.120.401749
815 75. Nonet ML. Rapid generation of *Caenorhabditis elegans* single-copy transgenes combining
816 recombination-mediated cassette exchange and drug selection. Genetics. 2023;224:
817 iyad072. doi:10.1093/genetics/iyad072
818 76. Nonet ML. Efficient Transgenesis in *Caenorhabditis elegans* Using Flp Recombinase-
819 Mediated Cassette Exchange. Genetics. 2020;215: 903–921.

820 doi:10.1534/genetics.120.303388
821 77. Ashley GE, Duong T, Levenson MT, Martinez MAQ, Johnson LC, Hibshman JD, et al. An
822 expanded auxin-inducible degron toolkit for *Caenorhabditis elegans*. Genetics. 2021;217:
823 iyab006. doi:10.1093/genetics/iyab006
824 78. Schwartz ML, Jorgensen EM. SapTrap, a Toolkit for High-Throughput CRISPR/Cas9 Gene
825 Modification in *Caenorhabditis elegans*. Genetics. 2016;202: 1277–1288.
826 doi:10.1534/genetics.115.184275
827 79. Paix A, Wang Y, Smith HE, Lee C-YS, Calidas D, Lu T, et al. Scalable and versatile
828 genome editing using linear DNAs with microhomology to Cas9 Sites in *Caenorhabditis*
829 *elegans*. Genetics. 2014;198: 1347–1356. doi:10.1534/genetics.114.170423
830 80. Paix A, Folkmann A, Rasoloson D, Seydoux G. High Efficiency, Homology-Directed
831 Genome Editing in *Caenorhabditis elegans* Using CRISPR-Cas9 Ribonucleoprotein
832 Complexes. Genetics. 2015;201: 47–54. doi:10.1534/genetics.115.179382
833 81. El Mouridi S, Peng Y, Frøkjær-Jensen C. Characterizing a strong pan-muscular promoter
834 (P*mlc-1*) as a fluorescent co-injection marker to select for single-copy insertions.
835 MicroPublication Biol. 2020;2020. doi:10.17912/micropub.biology.000302
836 82. Farboud B, Meyer BJ. Dramatic Enhancement of Genome Editing by CRISPR/Cas9
837 Through Improved Guide RNA Design. Genetics. 2015;199: 959–971.
838 doi:10.1534/genetics.115.175166
839 83. Ghanta KS, Mello CC. Melting dsDNA Donor Molecules Greatly Improves Precision
840 Genome Editing in *Caenorhabditis elegans*. Genetics. 2020;216: 643–650.
841 doi:10.1534/genetics.120.303564
842 84. Kamath RS, Fraser AG, Dong Y, Poulin G, Durbin R, Gotta M, et al. Systematic functional
843 analysis of the *Caenorhabditis elegans* genome using RNAi. Nature. 2003;421: 231–237.
844 doi:10.1038/nature01278
845 85. Moribe H, Yochem J, Yamada H, Tabuse Y, Fujimoto T, Mekada E. Tetraspanin protein
846 (TSP-15) is required for epidermal integrity in *Caenorhabditis elegans*. J Cell Sci.
847 2004;117: 5209–5220. doi:10.1242/jcs.01403
848 86. Ward JD, Mullaney B, Schiller BJ, He LD, Petnic SE, Couillault C, et al. Defects in the *C.*
849 *elegans* acyl-CoA Synthase, *acs-3*, and Nuclear Hormone Receptor, *nhr-25*, Cause
850 Sensitivity to Distinct, but Overlapping Stresses. PLoS ONE. 2014;9: e92552.
851 doi:10.1371/journal.pone.0092552.s013